BRNO UNIVERSITY OF TECHNOLOGY

VYSOKÉ UČENÍ TECHNICKÉ V BRNĚ

FACULTY OF MECHANICAL ENGINEERING

FAKULTA STROJNÍHO INŽENÝRSTVÍ

ENERGY INSTITUTE

ENERGETICKÝ ÚSTAV

FIBROUS AEROSOLS - METHODS FOR GENERATION, MEASUREMENTS, CLASSIFICATION AND FILTRATION

VLÁKNITÉ AEROSOLY – METODY GENEROVÁNÍ, MĚŘENÍ, TŘÍDĚNÍ A FILTRACE

MASTER'S THESIS

DIPLOMOVÁ PRÁCE

AUTHOR
AUTOR PRÁCE
Bc. Ema Liščáková

SUPERVISOR
VEDOUCÍ PRÁCE
doc. Ing. František Lízal, Ph.D.

BRNO 2025

BRNO UNIVERSITY OF TECHNOLOGY FACULTY OF MECHANICAL ENGINEERING

Assignment Master's Thesis

Institut:	Energy Institute
Student:	**Bc. Ema Liščáková**
Degree programm:	Power and Thermo-fluid Engineering
Branch:	Environmental Engineering
Supervisor:	**doc. Ing. František Lízal, Ph.D.**
Academic year:	2024/25

As provided for by the Act No. 111/98 Coll. on higher education institutions and the BUT Study and Examination Regulations, the director of the Institute hereby assigns the following topic of Master's Thesis:

Fibrous aerosols – methods for generation, measurements, classification and filtration

Recommended bibliography:

PAVELEK, Milan a Josef ŠTĚTINA. Experimentální metody v technice prostředí. 3. vyd. Brno: CERM, 2007. ISBN 978-80-214-3426-4.

HINDS, William C., 1999. Aerosol technology : properties, behavior, and measurement of airborne particles. 2nd. New York: Wiley. ISBN 0471194107.

Deadline for submission Master's Thesis is given by the Schedule of the Academic year 2024/25

In Brno,

L. S.

prof. Ing. Jiří Pospíšil, Ph.D. Director of the Institute	doc. Ing. Jiří Hlinka, Ph.D. FME dean

ABSTRAKT

Hlavným predmetom skúmania tejto diplomovej práce sú vláknité aerosoly. Teoretická časť popisuje vlastnosti vláknitých aerosolov, vrátane ich výroby, merania a klasifikácie podľa dĺžky vlákien. Experimentálna časť sa zameriava na klasifikáciu vláknitého aerosolu pomocou dielektroforézy, taktiež bola skúmaná závislosť kvality klasifikácie od rôznych vstupných parametrov, ako je relatívna vlhkosť nosného plynu, pomer prietokov v klasifikátore a rôzne amplitúdy aplikovaného napätia. Výsledky experimentov ukázali, že relatívna vlhkosť nosného plynu ma kľúčový vplyv na klasifikáciu nevodivých vlákien, zatiaľ čo zmeny aplikovaného napätia ovplyvňujú dĺžku klasifikovaných vlákien.

Kľúčové slova

vláknité aerosoly, dielektroforéza, klasifikácia vlákien, meranie vlákien, nevodivé vlákna

ABSTRACT

The main focus of this thesis is fibrous aerosols. The theoretical section covers properties of fibrous aerosols, including their manufacturing, measurement, and classification according to the length of fibers. The experimental part focuses on the classification of fibrous aerosol using dielectrophoresis, moreover, the influence of various input parameters on the quality of the classification, such as relative humidity of the carrier gas, ratio of flows within the classifier, and varying amplitudes of applied voltage, was studied. Results of conducted experiments conclude that the relative humidity of carrier gas plays a critical role in the classification of non-conductive fibers, while variations in applied voltage affect the length of classified fibers.

Key words

fibrous aerosols, dielectrophoresis, fiber classification, fiber measurement, non-conductive fibers

ROZŠÍRENÝ ABSTRAKT

Vláknité aerosoly ako predmet skúmania začal s hľadaním dôvodov problémov s dýchaním v miestach s výskytom azbestu. Správanie vlákien vo vznese vykazuje jedinečné aerodynamické vlastnosti. Avšak s eliminovaním využitia azbestu v stavebníctve, sa výskum zameral na pozitívne využitie vláknitých aerosolov a to na inhalovanie liečiv.

Teoretická časť sa najskôr zameriava na definíciu a popis aerosolov všeobecne a následne je pozornosť upriamená na vláknité aerosoly. Vláknité aerosoly sú špecifické tvarom častíc, ktoré obsahuje, a to v tomto prípade vláknami. Vlákno je definované ako častica, ktorej jeden rozmer prekračuje všetky ostatné aspoň trikrát. Tvar vlákna v skúmaní aerosolov predpokladá okrúhle telo s výraznou dĺžkou, a teda sa očakáva tvar valca alebo predĺženého sferoidu. Avšak toto je ich idealizovaný tvar, pretože sa vyskytujú rôzne deviácie od ideálneho tvaru, ako napríklad: rozštiepené konce alebo nepravidelnosti v priemere. Aj napriek nepravidelnostiam, vlákna sú popisované pomerom dĺžky k priemeru, a tento pomer sa nazýva fibrocita. Vlákna môžu byť z rôznych materiálov, ako napríklad už spomínaný azbest, ale aj sklo, plast taktiež aj súčasne veľmi využívané uhlíkové nanovlákna. Vlákna vďaka svojmu špecifickému tvaru, majú jedinečné aerodynamické vlastnosti. Pohyb vlákien je ovplyvnený ich polohou voči smeru prúdenia. Pohyb paralelne a priečne voči prúdeniu je ovplyvnený rôznym odporom a krútiacim momentom.

Vytváranie vlákien mikroskopických rozmerov predstavuje istú výzvu. Gilberston et al. (2005) skúmali generovanie mikroskopických vlákien pri usadzovaní z postranného uhlu. Týmto spôsobom sa formujú častice o malých rozmeroch, ktoré je možné oddeliť od filmu, na ktorom sú vytvárané pri ponorení do etanolu. Takto vytvorené vlákna boli aerosolizované pomocou prúdového nebulizéru. Následne ďalšia technika pre vytváranie netkaných vlákien je elektrostatické zvlákňovanie, ktoré dokáže vytvárať vlákna s rôznym priemerom v závislosti od použitého materiálu a nastavenia špecifík pri zvlákňovaní. Avšak elektrostatické zvlákňovanie produkuje dlhé a hlavne zamotané vlákna, preto je ich potrebné vhodným spôsobom narezať, aby bolo možné ich aerosolizovať (Thieme et. al. 2011). Biologicky rozložiteľné polyméry vytvorené elektrostatickým zvlákňovaním, je možné narezať v roztoku etanolu mechanickým spôsobom, za neustáleho chladenia tekutým dusíkom. Tento spôsob produkuje nasekané vlákna v dĺžkovom rozmedzí 5- 15 µm (Thieme et. al. 2011). Kryogenické mletie elektrostaticky zvláknených vlákien skúmal Verreck et al. (2003), kde bola dosiahnutá dĺžka vlákien približne 27 µm. Ďalšia z metód bola krátenie vlákien pomocou ultrazvuku, kde boli skúmané rôzne polyméry. Výsledkom boli vlákna polystyrénu s dĺžkou 10 µm, a pri použití vlákien z polymliečnej kyseliny, bolo dosiahnuté vlákien o dĺžke 40-50 µm, a nebola pozorovaná žiadna zmena priemeru. (Niemczyk-Soczynska et al. 2021)

Meranie vláknitých aerosolov zahŕňa hodnotenie tvaru vlákien, ako ich rozmerov ale aj chemického zloženia, ak ide o vlákna z neznámeho zdroja. Dôležitým prvkom pri pozorovaní aerosolov je zistenie či ide o vlákna alebo častice iných rozmerov. Štyri základné princípy pozorovania aerosolov sú tieto mikroskopovacie techniky: Mikroskop s fázovým posunom, mikroskop s polarizovaným svetlom, skenovací elektrónový mikroskop alebo transmitný elektrónový mikroskop. (Kulkarni 2011)

Klasifikácia vláknitých aerosolov, podľa rozmerov vlákien je zložitý proces, pretože neexistuje metóda, ktorá by zohľadňovala dĺžku a aj priemer vlákna súčasne. Väčšina popísaných metód rozdeľuje vlákna na základe ich priemeru, ako napríklad impaktory a cyklóny. (Kulkarni 2011)

Dielektroforéza je pohyb neutrálne nabitých častíc, pôsobením nehomogenného elektrického poľa. V častici dôjde k premiestneniu polarizačných nábojov, a teda nerovnosť náboja vnútri a vonku častice vyvolá pohyb. Dielektroforézu využil Baron et al. (1994) na zostavenie klasifikátora pre vláknité aerosoly. Medzi dvoma cylindrickými elektródami je

vytvorené nehomogénne elektrické pole. Vláknitý aerosol je privedený do priestoru medzi elektródami. Na zamedzenie usadenia vlákien na elektródy, sú privedené dva obalové prúdy medzi elektródy a prúd aerosolu, na zabezpečenie laminárneho prúdenia. Klasifikované boli azbestové vlákna rôznej dĺžky na základe rôzneho napätia, privedeného na elektródy. (Baron et al. 1994)

Elektroforéza, je pohyb elektricky nabitých častíc v elektrickom poli, a taktiež sa využíva pre klasifikáciu vlákien podľa ich dĺžky. Závisí na elektrickej mobilite, ktorá popisuje pohyb elektricky nabitej častice v elektrickom poli v smere danom znamienkom svojho náboja. Na dosiahnutie optimálnych výsledkov dĺžkovej klasifikácie elektroforézou je odporúčaná prvotná separácia vlákien podľa priemeru. (Han, Moss, Wong 1994)

V experimentálnej časti sa práca zameriava na dĺžkovú klasifikáciu vláknitých aerosolov podľa dielektroforézy, na základe štúdii od Barona et al. (1994)

Príprava sklenených vlákien, ktoré budú klasifikované, bol jeden z prvých krokov. Išlo o vlákna, ktoré vznikli lisovaním sklenej vaty Supafil® Loft určenej k izolácii. Po lisovaní boli sklenené vlákna zmiešané so sklenenou balotinou a následne preosiate cez sitá, aby sa dosiahla rovnomerná distribúcia vlákien v obsahu zmesi, a taktiež aby sa predišlo vzniku zhlukov vlákien. Meracia trať pozostávala z nasledujúcich častí: násypka so zmesou vlákien a balotiny, rotačný podávač, ktorý zabezpečoval kontinuálny posun zmesi. Zmes pokračovala do orbitálnej trepačky, ktorej pohyb vytváral fluidnú vrstvu, teda oddeľovala ťažšiu balotinu od vlákien, a tým vznikal vláknitý aerosol. Nosný plyn pre vznik aerosolu bol vlhčený vo zvlhčujúcej komore a jeho prietok bol kontrolovaný na prietokomeroch, pretože bolo nutné zabezpečiť rôzne prietoky pre obalové prúdy a prúd s aerosolom. Elektrické pole bolo vytvárané generátorom funkcií a následne zosilené zosilovačom, aby dosiahlo hodnoty v kilovoltoch. Aerosol z trepačky bol vedený cez neutralizátor aby sa vlákna zbavili nežiadúceho statického náboja. Aerosol bol privádzaný do klasifikátora z vrchu ako aj jeden obalový prúd, druhý obalový prúd bol privádzaný zospodu a bol vedený vnútornou elektródou hore. Klasifikovaný aerosol, s požadovanou dĺžkou vlákien, bol odvádzaný z dola klasifikátoru ako aj odpadný aerosol s časticami o nežiadúcom rozmere.

Vzorky vlákien boli zachytené na membránový filter, ktorý bol pred pozorovaním rozpustený výparmi acetónu. Takto pripravená vzorka bola pozorovaná pod mikroskopom s fázovým posunom a vlákna boli manuálne počítané. Na počítanie vlákien bola použitá Walton- Beckettova mierka, ktorá bola implementovaná v jednom z okulárov v mikroskope. Počítanie vlákien vyžaduje postupovanie podľa metodológie, ktorá je popísaná v *NIOSH* 7400 (2019). Medzi hlavné zásady počítania vlákien patrí: počítanie vlákien aspoň na 20 oblastiach z filtru a počítanie vlákien iba v rozsahu mierky. Táto metóda je určená najmä na určenie celkového počtu vlákien, avšak v tejto práci bolo potrebné zisťovať aj dĺžku vlákien, teda boli merané aj ich rozmery.

Hlavným zámerom práce bolo sledovať vplyv meniacich sa vstupných parametrov na klasifikáciu. Pozorované veličiny boli: zmena relatívnej vlhkosti nosného plynu, pomer obalových prúdov voči aerosolu a zmena napätia.

Efektivita klasifikácie pomocou dielektroforézy závisí na elektrickej vodivosti vlákien. Sklenenné vlákna sú prirodzený izolant, a teda je nutné dosiahnuť dostatočnú vodivosť pre klasifikáciu. Avšak väčšina častíc schopných vzletu, sa dá pokladať za vodivé, vďaka adsorpcii vody na ich povrch. (Fuchs, Davies 1989). Adsorpcia vody na povrch vlákien vyvolá zmenu povrchovej vodivosti, ktorá bude dostatočná na klasifikáciu dielektroforézou.

Závislosť klasifikácie na relatívnej vlhkosti bola experimentálne skúmaná, a to tak, že bola kontrolovaná vlhkosť nosného plynu pomocou ventilu. Vlákna sa začali klasifikovať pri relatívnej vlhkosti vyššej ako 25 %, a vyhovujúce podmienky boli dosiahnuté pri vlhkosti nosného plynu nad 40 %.

Ako ďalší vstupný parameter ovplyvňujúci kvalitu klasifikácie, bol pomer obalových prúdov voči prúdu aerosolu. Deye et al. (1999) tvrdia, že zmenšenie vnútorného obalového prúdu významne ovplyvňuje minimálnu klasifikovateľnú dĺžku vlákien, avšak zvyšuje dĺžkovú distribúciu vlákien. Toto tvrdenie sa nepodarilo dokázať, pretože pri počítaní vlákien, sa pre vysokú časovú náročnosť, vlákna kategorizovali do dĺžkových skupín. Nebolo teda možné vyhodnotiť, či nastalo zníženie minimálnej klasifikovanej dĺžky spolu so zvýšenou dĺžkovou distribúciou.

Závislosť klasifikovanej dĺžky na napätí, je indikovaná rovnicou (11). Z tejto rovnice môžeme vidieť že rýchlosť prúdenia vlákna v elektrickom poli, napätie privedené na elektródy a dĺžka vlákien sú jediné premenné, pretože ostatné konštanty popisujú vlastnosti buď vlákna, alebo prostredia, ktoré ostávajú nemenné. Z grafu závislosti dĺžky vlákna a napätia je zjavné, že tieto dve veličiny sú nepriamo kvadraticky úmerné, teda pri vyššom napätí sú klasifikované kratšie vlákna. Napätie privádzané na elektródy bolo od 0,8 kV po 4 kV, a následne boli klasifikované vlákna od 60 do 10 μm. Vyššie napätie nebolo nutné aplikovať, pretože vlákno o dĺžke 10 μm je už v minimálnych rozmeroch vlákna, keďže kratšie vlákno ako 9 μm by nesplňovalo definíciu vlákna, pretože skúmané vlákna mali priemer 3 μm. Tieto výsledky boli porovnateľné s výsledkami Wang et al. (2005). Hoci vlákna ich štúdii mali priemer iba 1 μm, hodnoty napätia a klasifikovanej dĺžky sa zhodovali. Zmena napätia pri najkratších vláknach požadovala najväčšie zmeny amplitúdy napätia, keďže pre zmenu klasifikovaných vlákien z 10 na 20 μm bolo potrebné znížiť napätie o 2 kV. Pre zmenu klasifikovanej dĺžky z 30 na 60 μm stačilo znížiť napätie o 600 V.

Výsledkom tejto diplomovej práce je zhodnotenie vstupných parametrov na kvalitu klasifikácie vláknitých aerosolov. Klasifikácia s využitím nehomogénneho elektrického poľa môže byť využitá pre vlákna s nízkou elektrickou vodivosťou akým je sklo a prípadne polyméry a biologicky rozložiteľné vlákna, ktoré majú svoje využitie v medicíne, konkrétne v aplikácii liekov priamo do pľúc.

BIBLIOGRAFIC CITATION

LIŠČÁKOVÁ, Ema. *Fibrous aerosols - methods for generation, measurements, classification and filtration*. Online, master's Thesis. František LÍZAL (supervisor). Brno: Brno University of Technology, Faculty of Mechanical Engineering, 2025. Available at: https://www.vut.cz/en/students/final-thesis/detail/165919. [accessed 2025-05-23].

DECLARATION

I declare that I have written this Master's Thesis on the subject **Fibrous Aerosols – methods for generation, measurement, classification and filtration** myself, with all sources and literature acknowledged in the bibliography.

23.5.2025	
Date	*Ema Liščáková*

ACKNOWLEDGEMENT

First and foremost, I would like to express my sincere gratitude to my supervisor, doc. Ing. František Lízal, Ph.D., for his support, valuable guidance, and encouragement throughout the course of my thesis. I am also thankful to Ing. Jana Kánska for her willingness to help in the laboratory. Last but not least, I would like to thank my family for their support during my studies.
This work was supported by projects GA22-20357S Measurement and computational simulation of transport of fibrous aerosols in high velocity gradient flow and interaction of fibres with a wall and CZ.02.01.01/00/22_008/0004634 OP JAK MEBioSys - Mechanical engineering of biological and bio-inspired systems.

Contents

1 Introduction

Fibrous aerosols have been the subject of extensive scientific investigation due to their unique aerodynamic properties and associated health risks. The research emerged largely as a response to health concerns related to asbestos, as its elongated shape poses significant health risks due to its ability to penetrate deep into the respiratory system. Following the regulatory restrictions on asbestos in the late 20th century, scientific interest in fibrous aerosols continued, as microfibers and nanofibers composed of materials such as carbon, glass, and polymers became crucial to many technologies. (Baron 2001) The distinctive morphology of fibers, particularly their length, influences the aerodynamic behavior and deposition patterns. Accurate classification of fibrous aerosols based on fiber length is therefore essential for risk assessment, industrial safety, and regulatory compliance. (Kulkarni 2011)

This thesis aimed to classify fibrous aerosols based on fiber length, with a focus on evaluating the influence of key input parameters on classification quality. Evaluation of the efficiency and reliability of different classification parameters under varying conditions, such as airflow ratio, electric field strength, in the case of dielectrophoretic separation, and humidity levels. Through an analysis of these factors, this thesis offers valuable insights for optimizing fiber classification by dielectrophoresis to enhance accuracy and reproducibility.

2 Aerosols

Aerosol is a system comprised of two phases, consisting of solid or liquid particles dispersed and suspended within a surrounding gas phase. Aerosols can be described as ubiquitous (Kulkarni 2011). The term aerosol encompasses many different types of aerosols; the most commonly named are dust, fume, smoke, mist, and others. Since the term aerosol includes many different types of aerosols, various systems of aerosol categorization exist. The subdivision of aerosols is determined mainly by the physical characteristics of particles and their mechanism of generation. The most significant characteristic of aerosol behavior is the particle size, as it affects all aerosol properties, such as its motion. The smallest particles are transported by Brownian motion, larger particles are affected by gravitational and inertial forces. The size distribution of suspended particles categorizes aerosol into two main categories: polydisperse aerosol, with a broad range of particle sizes, and monodisperse aerosol, with all particles of the same size. Though monodisperse aerosols are created by laboratory use, polydisperse aerosols are the only ones occurring naturally. The phase of the particles also impacts the shape of the particle, as liquid particles are almost always spherical, forming droplets. Alternatively, solid particles are generally formed into intricate shapes. Due to the wide spectrum of particle sizes, there is an emphasis on the prioritization of a microscopic approach and the analysis of individual particle properties. Non-spherical particles are categorized by multiple definitions of size and shape in an effort to correspond to the most relevant properties. Although most theoretical approaches presume the spherical shape. To enable such presumption, it is necessary to utilize correction factors and equivalent diameters. (Hinds, Zhu 2022)

Stricter regulations aimed at reducing particulate matter pollution are increasing the need to implement more time-consuming and resource-intensive measurements. Accurate assessment of the physical and chemical properties of aerosols affects the appropriate moderation. Aerosol measurement techniques generally fall into two categories: Collecting aerosol particles on a filter or substrate for later laboratory analysis, and in situ measurements, which provide near-real-time data. (Kulkarni 2011)

Fibrous aerosols are a category of aerosols characterized by their specific suspended particles, which are elongated, simply known as fibers. These aerosols exhibit distinct properties, such as unique aerodynamic characteristics and prolonged suspension times, necessitating specialized research methodologies. While fibrous aerosols are typically polydisperse, there is ongoing research on ways to generate a monodisperse fibrous aerosol and focus on characteristics that are mainly influenced by the length of the fiber. (Kulkarni 2011)

3 Fibers

Particles, whose shape can be described as non-spherical, particularly those with a prolonged shape or with one dimension notably more significant than the other two, are generally classified as fibers. Fibers are typically formed as a result of the manipulation and production of materials with a fibrous structure. Alternatively, fibers can be produced by spinning, which is a process of creating fibers from liquid solutions or melts (Greiner, Wendorff 2007). Fibers can also result as a side product when non-fibrous materials are subjected to stress. Additionally, the crystallization of certain organic materials can also produce fibrous particles. Numerically, fibers are within the microscopic scale, up to several hundred micrometers lengthwise. The size range of fibers is influenced by the type of bulk material and by the method of comminution of the bulk material. The inconsistency between length and diameter poses a challenge for precise size distribution measurement. (Kulkarni 2011)

3.1 Fiber Shape

Fiber shape is often assumed to be a cylinder or prolate spheroid, characterized by two key dimensions: length and diameter. Another specification, *β,* represents the ratio of length and diameter, defining fibrocity, also known as aspect ratio. Nevertheless, fibers often deviate from ideal shape assumptions, such as being straight and of comparable diameter throughout their length. Chemical composition also influences the fiber shape, as many fibers from various materials vary in their structure. Glass and mineral fibers are generally cylindrical, however, they may curve along their axis and may display irregular ends, mainly jagged or bulbous tips. Asbestos fibers, in particular, can split along their axis, producing progressively thinner fibers, known as fibrils. These fibrils may also display several degrees of splaying, splitting, curving, and a non-circular diameter of about 0,03 µm. When the asbestos mineral undergoes mechanical fragmentation, the material separates predominantly along the fibrils, producing fibers composed of bundles of fibrils. The ends can display further disaggregation into smaller bundles of fibrils, either fully detached or remaining at the end of the fibers but dispersed. (Kulkarni 2011)

Additionally, complex structures can be generated by a combination of multiple fibers and compact particles. Compact particles attached to the fibers impact the aerodynamic behavior. The intricate geometries of fibers influence all measurement techniques, often complicating direct comparison between different methods. Measurement techniques should be adapted to account for the size distribution and physical and chemical characteristics of the fibers. (Baron 2001).

Despite these variations in shape, length, and diameter are still the most representative characteristics of fibers. Fiber dimensions serve as a function of the behavior of the fibers suspended in a gas. It is suggested that the diameter often increases with length, as a result of the positive correlation between the natural logarithms of length and diameter of the fiber. Some fibers have been synthesized for toxicity assessments, others have been examined in environmental studies, and some have been created for calibration purposes. Therefore, comparisons of fiber size distributions from different analytical methods should be approached with caution. (Kulkarni 2011)

Carbon nanotubes (CNTs) and carbon nanofibers (CNFs) are utilized in a wide spectrum of fields, including the medical sector, electronic devices, various additives, and composites. CNFs occupy an intermediate position in terms of size between conventional milled carbon fibers, typically 5–10 µm in diameter, and single-walled carbon nanotubes (SWCNTs), which range from 1–10 nm in diameter. CNFs generally exhibit diameters in the range of 50–200 nm, lengths spanning from several tens of micrometers to multiple centimeters, and average aspect ratios exceeding 100. They also exhibit diverse morphologies, including cupped or stacked graphene configurations. The primary structural distinction between CNFs and CNTs lies in the orientation of the graphene planes. Generally, CNTs and CNFs can be distinguished by their structural characteristics, with the primary differentiating feature being that CNFs lack the continuous hollow cavity present along the entire length of CNTs (Bezemer 2006), as seen in Figure 1. Specifically, CNFs are identified by a misalignment between the graphene planes and the fiber axis, whereas CNTs are defined by a parallel alignment of these structural features. Structurally, CNTs share several similarities with multi-walled carbon nanotubes (MWCNTs), which can reach diameters up to 100 nm; both materials possess hollow cores and may present either as discrete entities or in bundled fibrous forms In contrast, SWCNTs are characterized by their less rigid structure and a pronounced tendency to aggregate into non-fibrous bundles or rope-like formations, as illustarted in Figure 2.(Evans, Ki 2010)

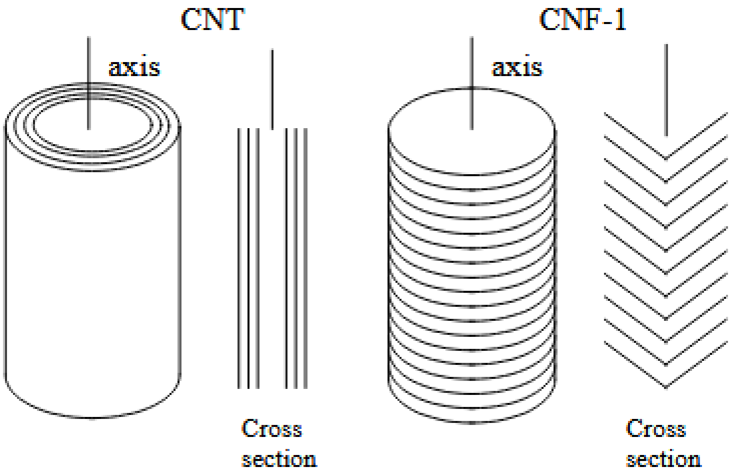

Figure 1: Structure of CNTs and CNFs (Bezemer 2006)

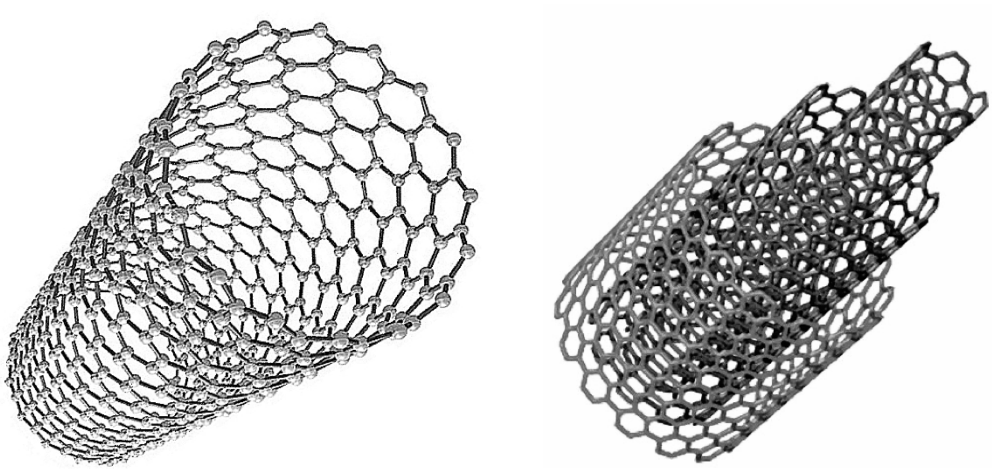

Figure 2: Structure of SWCNTs and MWCNTs (Goldmann, Górski, Klemczak 2021)

3.2 Fiber transport

Transport of the fibrous aerosols can be observed from two perspectives, microscopic and macroscopic. The physical properties of fiber influence the flow of the gas at a microscopic scale, which affects the drag forces acting upon them. Conversely, at the macroscale, overall gas flow governs particle transportation and deposition behaviour. To conclude, a comprehensive understanding of aerosol transport requires multiple points of view, meaning the fluid dynamics of the suspending medium and the particles' response to external force, and the particle-gas interaction. (Kulkarni 2011)

The transport behavior of fibrous particles exhibits orientation-dependent dynamics, governed by the alignment of the fiber's major axis relative to the direction of motion through the surrounding gas medium. The fiber axis can be oriented perpendicularly to the motion, illustrated in Figure 3a, or parallelly, Figure 3b. The motion is often described by a combination of the two orientations. (Kulkarni 2011)

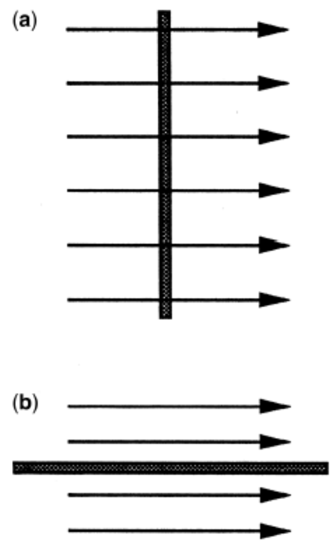

Figure 3: Fiber orientation a) Fiber aligned perpendicular to relative gas motion b) Fiber aligned parallel to relative gas motion (Kulkarni 2011)

The drag on a fiber is the greatest when it is oriented perpendicular to the flow of the surrounding gas. While the difference in the drag between the orientations is typically about 15-30 %, it can be difficult to determine the contribution of each orientation in the experimental system. At low Re_p (Reynolds number for particle), fiber orientation will be stable and will not change due to translational motion, e.g. gravitational force, but will drift somewhat due to orientation. Larger fibers, with Re_p greater than 0.01, will settle with their major axis oriented perpendicular to the direction of motion. With increasing $Re_p > 100$, $\beta > 20$ are still stable in the perpendicular orientation, but there is an increasing trend toward instability. (Kulkarni 2011) Equation (1) for aerodynamic diameter d_a of a prolate spheroid is given by Fuchs (Fuchs, Davies 1989)

$$d_a = d_f \sqrt{\frac{\rho_f \beta_a}{\rho_0 \chi}} \tag{1}$$

where, d_f is the physical diameter, ρ_f is the fiber density, and ρ_0 is the standard fiber density.

For motion parallel and perpendicular to the fiber major axis, the respective dynamic shape factors $\chi_{\parallel}$ and $\chi_{\perp}$ for prolonged spheroids are given by Fuchs (1989) by Equations (2) and (3) respectively (Fuchs, Davies 1989)

$$\chi_{\parallel} = \frac{4(\beta^2 - 1)}{3} \Big/ \left\{ \frac{2\beta^2 - 1}{\sqrt{\beta^2 - 1}} \ln\left(\beta + \sqrt{\beta^2 - 1}\right) - \beta \right\} \tag{2}$$

$$\chi_{\perp} = \frac{8(\beta^2 - 1)}{3} \Big/ \left\{ \beta^{1/3} \frac{2\beta^2 - 1}{\sqrt{\beta^2 - 1}} \ln\left(\beta + \sqrt{\beta^2 - 1}\right) + \beta \right\} \tag{3}$$

where β is fibrocity.

When subjected to velocity gradients, a torque is applied on the fiber until alignment parallel to the direction of shear is achieved. Consequently, when settling in a horizontal laminar flow, fibers are prone to be oriented horizontally, parallel to the applied shear force. However, sometimes a sudden motion described as a flip of the fiber is present, which is a periodic instability. This instability is influenced by both fiber dimensions and the magnitude of velocity gradients. Therefore, under such circumstances, the aerodynamic diameter cannot be considered solely an inherent particle property, as it becomes dependent on the experimental measurement parameters. The elongated shape of fibers makes interception during translational motion more significant for their deposition compared to compact particles. Nevertheless, shear flow often aligns the fibers, which lessens the impact of their length on interception. (Kulkarni 2011)

3.3 Fiber generation

Preparation of fibers for generating aerosols is a critical step in producing effective aerosols. Some fibers are available in a sufficiently comminuted state for direct use, while others require size reduction by grinding, chopping, or other methods. Various equipment, such as blenders and grinders, is utilized to ensure size reduction. (Kulkarni 2011)

3.3.1 Generation from thin films

Fibers for aerosolization can be generated from thin films as described by Gilbertson et al. (2005). Silica and titanium oxide fibers were produced by thin film fabrication, by glancing angle deposition (GLAD), which creates tiny, separated structures from thin film coatings, developed at the University of Alberta (Robbie, Brett 1997). Figure 4 displays fibers of titanium oxide, which were produced by GLAD. Throughout the deposition process, the substrates were spun around their normal axes while titanium was vaporized by an electron beam within a vacuum. A film thickness of 40 nm was deposited per rotation at a rate of 0.9 nm/s, totaling 50 complete rotations, which created the film of fibers. When immersed in ethanol and subsequently in an ultrasonic bath, individual fibers detached without cluster formation. The suspension of fibers was aerosolized by a jet nebulizer. However, this method did not produce a monodisperse aerosol, the fibers differed in length from 0,2 to 2,2 µm. Although the diameter and length of fibers produced by this method are strongly correlated and the longest fibers were 2 µm long and around 170 nm in diameter. Through the GLAD film deposition method, the morphology of nanoscale structures can be controlled, forming arrays of columns that project from the substrate. (Gilbertson et al. 2005)

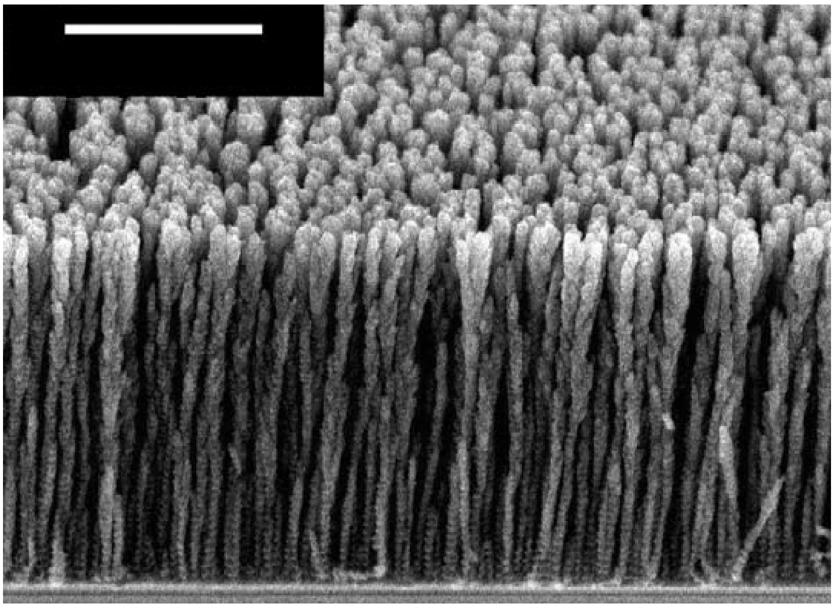

Figure 4: Thin film prepared by GLAD, scale represents 1µm (Gilberston et al. 2005)

3.3.2 Electrospinning

The one technique that grants the production of continuous fibers with consistent diameters that can be as thin as a few nanometers is known as electrospinning. Fibers can be produced from many materials, such as polymer alloys, synthetic and natural polymers, nanoparticles, moreover metals, ceramics. The diameter range fitting into the nanoscale is especially significant in biological systems, as it corresponds to the size range of proteins, viruses, and bacteria. A comparison, illustrated in Figure 5, of these biological structures with electrospun fibers reveals that the fiber diameters can vary considerably within this range. Electrospinning exhibits as a straightforward technique for producing fibers with diameters down to the nanometer scale, yet it requires careful control. (Greiner, Wendorff 2007)

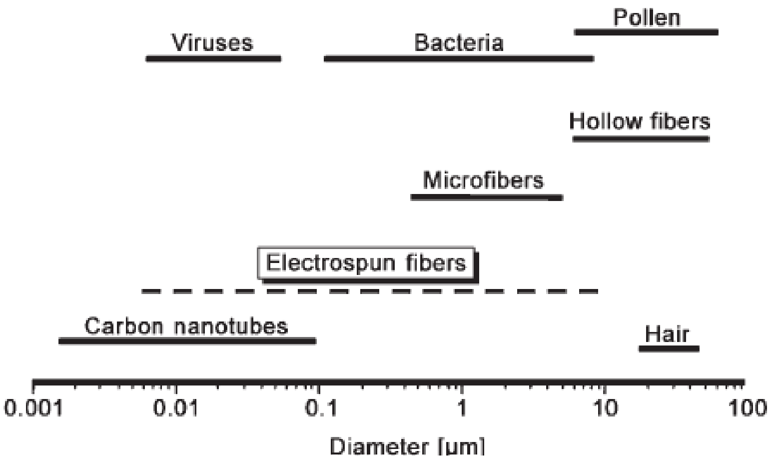

Figure 5: Comparison of diameters od electrospun fibers to those of biological and technological objects (Greiner, Wendorff 2007

The electrospinning layout consists of a nozzle, which concurrently operates as the distribution of the polymer solution, as well as an electrode of a high electric field of 100- 500 kV/m. A counter electrode is positioned 10 to 25 cm away, and the collection substrate, where electrospun fibers accumulate, is usually in contact with it, as illustrated in Figure 6. As the voltage is applied, a cone-shaped deformation forms at the polymer droplets' surface, known as the Taylor cone, with an angle of approximately 30°. The evaporation of the solvent or solidification of the melt occurs throughout its trajectory from the nozzle to the counter electrode. Solvent evaporation or melt solidification occurs, leading to the formation of solid fibers with diameters ranging from micrometers to nanometers. These fibers are deposited onto the counter electrode at high velocities 40 m/s or higher.

The characteristics of the fibers, created by electrospinnig, are influenced by various parameters, including the strength and geometry of the electric field, the feed rate of the polymer solution, and the properties of the substrate. Additionally, environmental factors such as the solvent's vapor pressure and the relative humidity of the surroundings can significantly effect fiber formation and also the individual properties of polymer, its molecular weight, molecular weight distribution, and solubility. Furthermore, the polymer solution characteristics, including viscosity, viscoelasticity, concentration, surface tension, and electrical conductivity. All play crucial roles in determining whether fibers or, in some cases, beads are formed. Fibers may also exhibit bead-like structures resembling pearls along their length. However, the formation of beads can be avoided by different spinning specifications. (Greiner, Wendorff 2007)

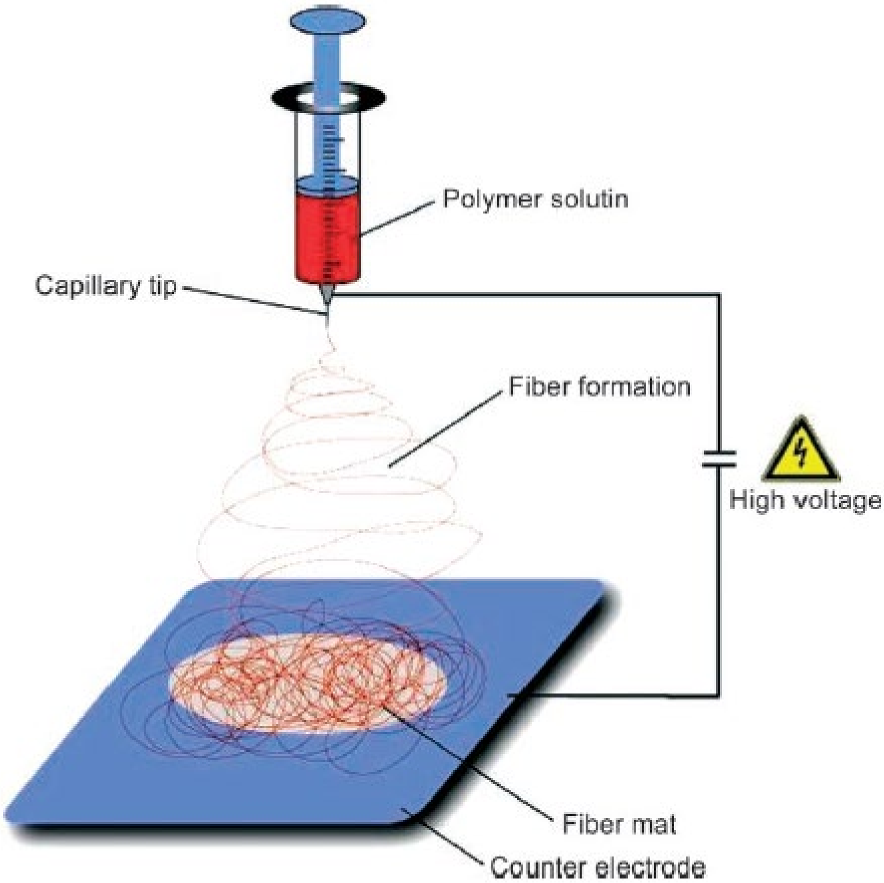

Figure 6: Electrospinning scheme with perpenidicular arangement of electrodes (Greiner, Wendorff 2007)

Greiner and Wendorff (2007) name two other methods for manufacturing thin polymer fibers: melt-blown and multicomponent processes. Both techniques are aplicable for thermoplastic polymers only and produce fibers with diameters below 500 nm. The melt-blown method involves pressing molten polymers through a series of nozzles under high pressure, with fibers solidifying rapidly as they cool. Multicomponent fibers, made from different polymer sections, are produced through extrusion processes, for instance, by water jets. Although these methods are more effective than electrospinning and can create fine fibers directly from the melts, electrospinning offers superior versatility, allowing precise control over fiber diameter and compatibility with a wide range of polymers. This makes electrospinning an essential technique for material nanostructuring. (Greiner, Wendorff 2007)

3.3.3 Cutting electrospun fibers

Bioerodible polymers can be synthesized into fibers by the process of electrospinning. However, as is the nature of the electrospun fibers, the formation yields long intertwined fibers. Mechanical cutting of electrospun fibers was carried out by Thieme et al. (2011). The fibers were synthesized from polyethylene oxide and DL-lactide by ring-opening polymerization to form multiblock copolymers with desired properties of biocompatibility and hydrophilicity. The formed poly(lactide-co-ethylene oxide) (PLA-PEO-PLA) copolymer was electrospun from 6, 8, and 10 wt% (weight percent) chloroform solutions, producing fibers. The voltage was adjusted between 15 and 30 kV, with a flow rate of 1 ml/hr and an electrode distance of 20 cm. However, 15 kV produced the highest-quality fibers. Overall, the fibers exhibited cylindrical structures with smooth, non-porous surfaces. The diameters of the fibers across all observed polymers ranged from 1 to 3 μm. An increase in polymer concentration generally led to larger fiber diameters. Fibers electrospun from 6 wt% solutions displayed noticeable diameter fluctuations along their length, whereas those produced from 8 and 10 wt% solutions were more uniform, as seen in Figure 7. (Thieme et. al. 2011)

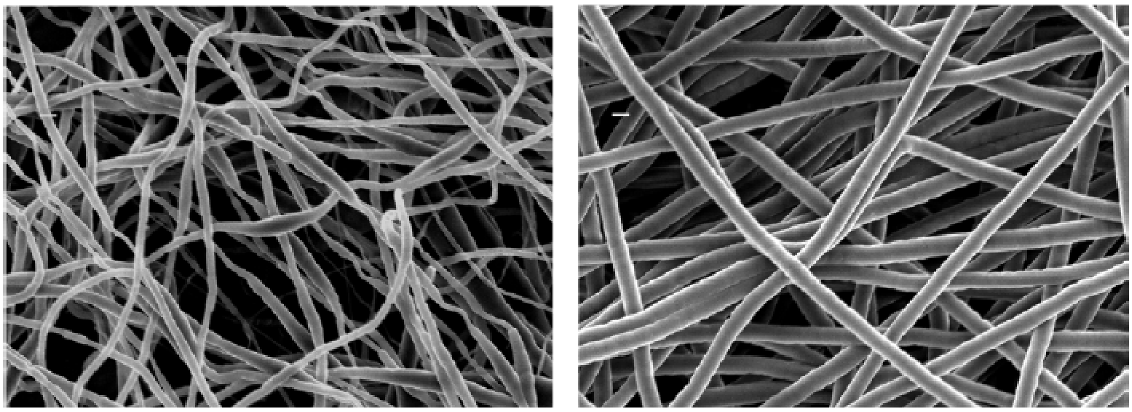

Figure 7:Fibers spun from different concentrations of 6 wt% and 10 wt% respectively (Thieme et. al. 2011)

The production of short-fiber electrospun mats was performed by mechanical cutting. The procedure was executed as follows: 200 ml of ethanol and 40 mg of electrospun fibers were cooled using liquid nitrogen until fully solidified. The cutting was performed using a motor- driven blade, operating at a speed of 26,000 turns/min for approximately 10 minutes. Following the cutting process, the fibers were separated from the cutting medium through centrifugation at 3,500 turns/min to ensure proper isolation and collection. The cut fibers, displayed in Figure 8, were within the intended size range of 5-15 μm, signifying that the process of mechanical cutting of electrospun fibers can be utilized in biomedical applications, especially in inhalation therapy of drug-loaded short fibers. (Thieme et. al. 2011)

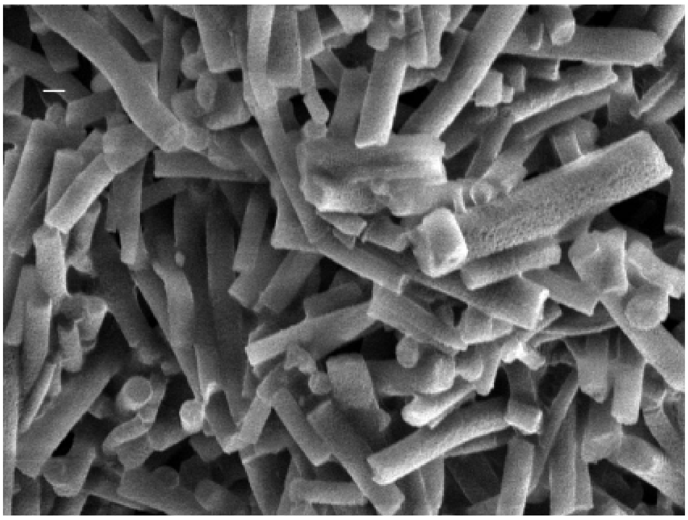

Figure 8: Cut fibers (Thieme et. al. 2011)

3.3.4 Cryogenic milling

Another method to gain short fibers from long electrospun fibers is cryogenic milling. The method was used by Verreck et al. (2003) to fracture fibers of water-soluble polymer hydroxylpropylmethylcellulose (HPMC) and the poorly water-soluble drug itraconazole to facilitate pharmaceutical applications. Solutions of different molecular weights of itraconazole/HPMC in ethanol/methylene chloride were spun at 16 kV and 24 kV, producing a long, intertwined web of nanofibers with a diameter in the range of 300 nm to 4 µm. Higher voltage 24 kV yielded thinner fibers 300–500 nm in diameter in comparison to 1 – 4 µm in diameter at 16 kV. Fibers were milled for 10 minutes using a cryogenic mill with liquid nitrogen used as a coolant. After milling, the fibers had an average length of approximately 27 µm. The technique offers a scalable approach to enhance the bioavailability of poorly soluble drugs, with potential applications in oral, topical, and controlled-release delivery systems. (Verreck et al. 2003)

3.3.5 Ultrasonication

Ultrasonication produces short electrospun fibers through a fragmentation process driven by bubble cavitation and implosion, which generate energy that causes fiber breakage (Sawawi et al. 2013). This method enables the rapid and straightforward production of short fibers from brittle materials. However, like most mechanical fragmentation techniques, ultrasonication results in a wide variation in fiber lengths, which can limit its applicability in certain fields.(Niemczyk-Soczynska et al., 2021)

Sawawi et al. (2003) showed that polymers' ductility affects the process of ultrasonication, as brittle polymers like polystyrene (PS) and poly(methyl methacrylate) (PMMA) were fragmented into short fibers approximately 10 µm long in a matter of seconds. The fragmentation of more ductile polymers like poly(L-lactide) (PLLA) and poly(acrylonitrile) (PAN) was challenging, and it was suggested that pre-treatment and prolonged time were necessary. Initial fiber alignment influenced the final fiber length. Smaller diameters and aligned fibers produced shorter, more uniform fibers. Aligned PS fibers yielded shorter lengths, approximately 3 µm long, compared to randomly oriented fibers, which were around 6 µm long. The chemical composition and physical morphology of the fibers remained stable during the ultrasonication process. Compared to cryogenic milling of these polymer fibers, ultrasonication was more effective in producing short fibers because cryogenic milling produced flakes and fibers, not uniform short fibers. (Sawawi et al. 2013)

Furthermore, Niemczyk-Soczynska et al. (2021) focused on improving the production of poly(l- lactide) acid (PLLA) fibers. Electrospun fibers were fabricated from PLLA with varying molecular weights. The conglomerate of electrospun fibers was pieced into 1 mm^2 cuts and submerged into a sonication medium consisting of demineralized water and isopropanol. Ultrasonic fragmentation was performed by an ultrasonic homogenizer at 26 kHz. The total operation time varied between 30 and 60 minutes with a sonication cycle of 1 second on and 1 second off, with the amplitude of 90-98 %. Two different processes were utilized to remove fibers from the solution after fragmentation. The fiber-containing medium was either filtered through 40 µm cell strainers to achieve a more uniform fiber length distribution or poured directly onto a foil under a fume hood to allow for solvent evaporation. Filtration through 40 µm filters following fragmentation further minimized fiber length distribution and the coefficient of variation by eliminating longer fibers. The study displays that ultrasonication can efficiently reduce the length of oriented electrospun PLLA fibers. While this method does not alter the polymer's molecular weight, it does influence the crystallinity of PLLA fibers. The efficiency of ultrasonic fragmentation is not dependent on polymer molecular weight after prolonged fragmentation. A stable fiber length was nearly achieved after 40 minutes of ultrasonication, ranging between 58 and 70 µm. Furthermore, the length range of filtered fibers was between 40 and 50 µm. Figure 9 displays different stages of PLLA fibers. No statistically significant result was found on the relation between fiber diameter and ultrasonication time and its impact on fiber diameter. (Niemczyk-Soczynska et al. 2021)

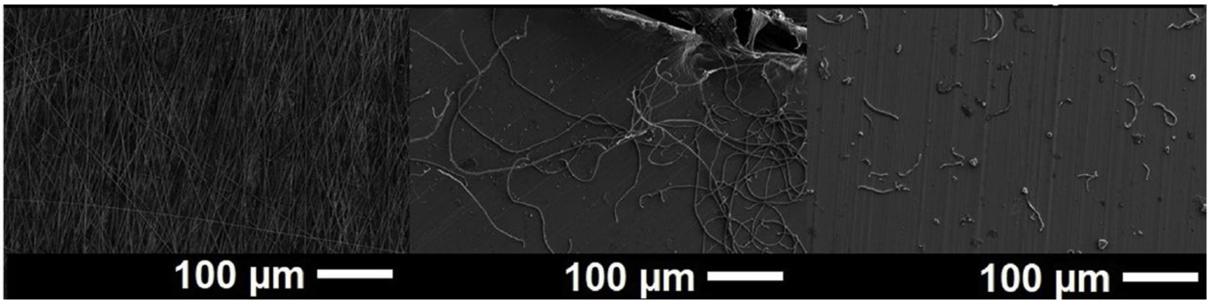

Figure 9: PLLA fibers a) after electrospinning, b) after ultrasonication, c) after filtration (Niemczyk-Soczynska et al. 2021)

3.4 Generating fibrous aerosols

Spurny names two main methods for generating fibrous aerosols: the vibrating bed generators and suspension generating equipment. The operation of a vibrating bed aerosol generator (VBAG) relies on the vibration frequency, amplitude, and gas flow rate after the dried fibrous material is introduced into the system. The concentration and size distribution of the generated aerosol are influenced by the physical dynamics within the fluidized bed, particularly the mechanical vibrations acting on fiber agglomerates. Due to the high porosity of the bed, the fibrous powder remains in a fluidized and disintegrated phase, minimizing bonding forces between individual fibers and allowing their dispersion through the gas flow. The cohesiveness between fibers is primarily dependent on fiber length, requiring stronger vibrations for the effective dispersion of longer fibers. By adjusting vibration parameters, both fiber concentration and size can be precisely controlled. However, the VBAG is generally limited to generating fibers with diameters of 0.5 µm and larger, and the initial fiber size distribution within the bed remains a critical factor in the process. (Spurny 1999)

To generate aerosol consisting of very sparsely dispersed fine fibers, a specialized generator designed for dispersing liquid suspensions of fine fibers must be used. This process involves mixing distilled water and methyl alcohol with extremely fine fibers, such as chrysotile asbestos, and subjecting the solution to ultrasonic treatment. The generated microdroplets are then dried using silica gel and activated charcoal columns. Maintaining sufficient dilution of the starter fibrous-liquid mixture is essential to minimize aggregation and ensure the dispersion of individual fibers. (Spurny 1999)

Typically, fluidized bed systems are characterized by two coexisting phases: a solid powder phase, comprised from one or multiple components, and a flowing air phase that moves through the particulate matter. The powder phase may consist solely of the material to be aerosolized or may include larger beads that are too heavy to be carried by the airflow. These larger particles are utilized to promote the separation of powder particles and prevent the creation of agglomerates. It has been observed that highly charged fibers are produced when fluidized beds are operated with dry air. However, when the relative humidity of the air is increased to approximately 15%, the charge level is reduced by nearly ten times. (Kulkarni 2011)

3.5 Fiber health effects

Even though fibers are commonly used in many fields, there is a negative condition linked to their occurrence, like the fact that exposure to fibrous aerosols causes diseases. The research connecting diseases to fiber exposure started with asbestos, and it was found that at least three types of illnesses are related to asbestos exposure. Asbestosis, which is a scarring of the lung tissue, mesothelioma, which is a cancer of the inner membrane of the lungs and the inner membrane of the abdominal cavity, and lung cancer. Along with fiber chemistry and solubility in the body, their physical shape appears most significant. Respiratory deposition patterns show why fiber diameter matters in the disease breakout. Only particles below 2-3 μm can reach the thoracic region, while alveolar penetration demands even smaller diameters. It has been suggested that short fibers possess substantially lower pathogenic potential, as they can be efficiently phagocytosed and cleared from the lungs by alveolar macrophages. In contrast, longer fibers resist complete internalization by these immune cells, resulting in their prolonged persistence within lung tissue and an increased risk of pathogenic effects. (Kulkarni 2011)

While asbestos is a well-documented hazardous fiber, it is not the only one of concern. With the growing production of carbon fibers, research attention has increasingly shifted toward investigating their potential health impacts. The likelihood of respiratory exposure to fibrous carbon nanomaterials is dependent upon production procedures, material handling protocols, and their inherent susceptibility to aerosolization. Given the extensive variety among CNTs and CNFs types, each exhibiting distinct morphological and compositional properties. Thus, the characterization and accurate evaluation of potential inhalation hazards remain inherently complex. (Ku, Birch 2019)

Several toxicological investigations have concentrated on SWCNTs and MWCNTs. Exposure to SWCNTs has been associated with a range of adverse pulmonary effects, including inflammation, rapid onset of pulmonary fibrosis, oxidative stress, mutagenesis, and dermal inflammation. Notably, concerns have emerged regarding the potential asbestos-like pathogenicity of MWCNTs. More recent findings indicate that CNFs may similarly elicit acute inflammatory responses and early-stage pulmonary fibrosis following pharyngeal aspiration exposure. (Evans, Ki 2010)

3.5.1 Health protection

There are several critical health protection strategies to minimize occupational exposure to fibrous aerosols. The strategies can be divided into two categories: personal health protection and reducing aerosol production. Together, these measures aim to reduce the risk of inhalation and dermal exposure to CNFs, which have been associated with respiratory issues and other adverse health effects. Evans, Ki, (2010) suggested various solutions for reducing the production of fibrous aerosols during the process of producing carbon nanofibers. The first suggestion was a solution to reduce dust production during the collection of the product, to include a continuous liner offloading system that encloses dust and a ventilated bagging station. Another solution is to enclose the product transfer system in a way that includes sealing the drum or bag to the filling vessel and using a continuous liner-type bagging system. The next significant improvement is adding a local exhaust ventilation near the bagging station can help capture airborne CNFs, though the exhaust flow must be optimized to ensure effective containment without significant product loss. To prevent the emission of ultrafine fibers, which are produced during thermal treatment, it is necessary to take precautions. To provide a fully coated system that would ensure the capture of these particles would be challenging, so the best strategy is to install a full or partial ventilated enclosure or use a canopy hood. Since the particles are primarily ultrafine with low inertia, gas/vapor-type capture velocities may be adequate. These methods, commonly used in other industries, can effectively minimize CNF exposure when properly designed and implemented. In addition to engineering controls, the study recommends administrative measures to further reduce risk, including limiting worker access to high-exposure areas and optimizing task scheduling to minimize the number of exposed personnel. (Evans, Ki 2010)

Personal protective equipment, especially respiratory protection and protective clothing, is advised. Regular monitoring using direct-reading instruments is encouraged to track airborne particle levels, assess control effectiveness. Moreover, routine maintenance of control systems and comprehensive worker training on the hazards of CNFs and safe handling procedures are emphasized as integral components of a comprehensive health protection program. (Evans, Ki 2010)

4 Measurement techniques

Understanding aerosols requires detailed analysis of their morphology, including size and shape, as well as their chemical composition. Advanced single-particle analysis techniques provide the most effective means of obtaining this information. In specific applications, such as identifying and measuring fibrous aerosols, these methods are particularly essential. Fibrous aerosols of anthropogenic origin are commonly found in workplaces, indoor spaces, and outdoor environments, where they are present as a mixture of various other aerosols. As a result, it is crucial to use analytical techniques that can accurately differentiate between fibrous and non-fibrous particles. The most effective approach is to directly observe the shape of individual particles using microscopic techniques or to identify the particles indirectly by light scattering. An optimal strategy for measuring and identifying fibrous aerosols involves combining electron microscopy with single-particle analysis. (Spurny 1999)

Sampling of fibers utilizes interception on filter substrates, which are further analyzed. Kulkarni (2011) names four main types of microscopes applied for fiber analysis: the phase contrast light microscope (PCM), the polarized light microscope (PLM), the scanning electron microscope (SEM), and the transmission electron microscope (TEM). Depending on the levels of precision imposed by the necessary analysis can be executed within different scopes of methods, such as quantitative enumeration as well as qualitative assessment of fiber characteristics. Following the regulation, inspecting the number of fibers and qualitative analysis is valued as the most efficient approach. However, if the fiber sources are unspecified, whether as part of research or an environmental evaluation, determining the complete size distribution and qualitative analysis of individual fibers may be compulsory. (Kulkarni 2011)

A critical aspect of adequate microscopic observation is sample preparation, as only a limited portion of the sample is examined. The visualization of fibers is predominantly two- dimensional. Therefore, it is essential to ensure a uniform distribution of the particles at the optimal concentration or deposition density across the sample surface. Excessive loading can lead to overlapping fibers and particles, complicating the analysis, whereas insufficient loading may result in extended search times to locate an adequate number of observable particles. Overestimation of fiber concentration may be caused by low filter loading, as a result of higher fiber visibility on a clear background. However, it was indicated that particles shorter than 2–3 μm are often misclassified as non-fibrous due to insufficient resolution, potentially leading to underestimation of fibrous aerosol concentrations. (Kulkarni 2011)

4.1 Phase Contrast Microscopy

Concentrations of airborne fibers are the most widely monitored by PCM, as it provides cost-effective results relatively quickly. PCM is an interferometric technique, allowing low-contrast particles to be viewed. By generating an interference pattern from both phase-shifted and unshifted light, PCM converts phase differences into intensity variations, which can then be detected. Light passing through the object undergoes a phase shift relative to that transmitted solely through the substrate, though this shift remains imperceptible to the human eye. Fibers are collected on filters from cellulose. After collection, the filter is chemically cleared and mounted on a glass slide for examination. Using a phase contrast microscope at approximately 450× magnification, fibers are counted within predefined observation fields outlined by a Walton-Beckett graticule, as illustrated in Figure 10. For statistical reliability, between 20 and 100 fields are typically analyzed. The resolution of PCM depends on several factors, including the optical properties of the microscope, the wavelength of light, and the refractive index contrast between the object and its surrounding medium. Accuracy in fiber counting is subject to bias and variability, with a relative standard deviation of 10% expected under optimal conditions, including uniform sample deposition, minimal background interference, and appropriate fiber loading. However, additional sources of variation, such as limited sample size or microscopist subjectivity, may further impact measurement precision. (Kulkarni 2011) Due to the inherent limitations of light microscopy, the method is unable to detect all fibers. As a result, it serves only as an index of exposure, based on the assumption that the detected fibers are representative. Nevertheless, PCM gained widespread use due to its low equipment costs and the minimal training required for conducting analyses. (Baron 2001)

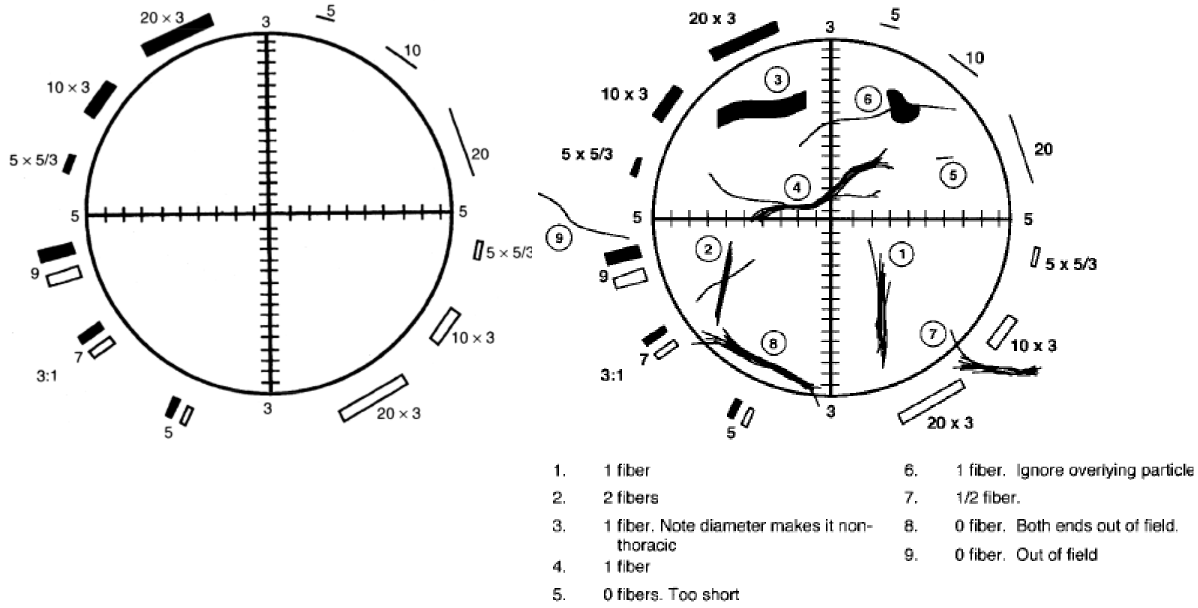

Figure 10: a) empty Walton-Beckett graticule (Kulkarni 2011) b) graticule with fibers that are countable and uncountable (Baron 2001)

4.2 Polarized light microscopy

Polarized light microscopy serves as a tool for identifying sources of aerosols, such as airborne fibers. Dispersion staining is a technique that utilizes the wavelength-dependent dispersion properties to detect the refractive indices of transparent particles. A particle immersed in oil with a similar refractive index and exposed to white light, the particle exhibits a distinct coloration due to the different dispersion of light as it propagates through both the particle and the immersion medium. This observed coloration, known as the dispersion color, serves as a diagnostic tool for identifying the particle's refractive index by comparing it with the colors observed in glass particles of known refractive indices placed in the same immersion oil. Another technique is index-matching, where an index of refraction is concluded by submerging particles in a sequence of mounting oils or temperature-varied oils. The index of refraction of the particle is the one that is the least visible in the index of refraction of the oil. Both techniques yield highly accurate results when executed properly. Furthermore, certain wavelengths of light may be selectively absorbed by a particle, resulting in a characteristic color when viewed under bright-field illumination. This property can provide the information needed for material identification. If the observed color varies depending on the direction of light propagation, the particle is described as exhibiting pleochroism. The identification of fibers based on their distinct optical properties under polarized light is feasible only for fibers exceeding 1 µm in width, whereas finer fibers are typically identified indirectly by analyzing larger, distinguishable fiber bundles. (Kulkarni 2011)

4.3 Scanning electron microscopy

Scanning electron microscopy offers an intermediate level of resolution. Various devices in this category were incapable of detecting all fibers. However, modern SEM systems have been developed with the capability to identify fibrils. Additionally, energy-dispersive X- ray (EDX) analysis, commonly available in SEMs, provides qualitative insights into fiber composition. In SEM imaging, particles are visualized by directing a focused electron beam onto the sample surface, which is then scanned across a defined area. An image of the scanned region is generated by synchronizing dispersed electrons with the beam scan rate. As a result, SEM analyzes the surface of particles on a substrate. Optimal imaging is achieved when conductive objects are placed on a smooth, conductive substrate. Typically, particles are deposited on aluminum or carbon planchets, which can be directly inserted into the SEM, or on polycarbonate membrane filters. To enhance conductivity, samples are often coated with gold or carbon. Several SEM-based methods have been developed for fiber counting. These techniques are mainly applied to inorganic man-made fibers, which generally have larger diameters. (Baron 2001)

4.4 Transmission electron microscopy

The most advanced technique for fiber counting and analysis is transmission electron microscopy (TEM), with the capability to detect even the smallest fibers, such as carbon nanotubes and asbestos fibrils. In addition to fiber detection, TEM enables the detection of crystal structure through electron diffraction and elemental composition using energy-dispersive X-ray analysis. While TEM offers high precision, factors such as sample collection, preparation procedures, and the complexities of analysis can affect the accuracy of the results. (Baron 2001)

For TEM analysis, airborne fiber samples are usually collected on a filter, commonly a polycarbonate membrane or a mixed cellulose ester (MCE) membrane. The two methods of the transfer approach of filters commonly used are the direct and indirect methods. The direct-transfer approach preserves the spatial arrangement of fibers as they were collected. The MCE filters are chemically collapsed to create a smooth surface that confines collected fibers. A carbon film is then applied to encapsulate the exposed fibers, after which the filter material is dissolved, leaving the carbon film intact. This film is subsequently transferred onto a TEM grid for analysis. The indirect-transfer technique involves dissolving the entire filter in liquid, followed by ultrasonic dispersion to separate particles. A portion of this suspension is then deposited onto a polycarbonate filter before final transfer to a carbon film. While the indirect approach allows for optimal particle loading and the removal of soluble particles, the dispersion process may alter the apparent size distribution of particles and fibers, potentially breaking apart fiber agglomerates or even fragmenting fibers into smaller fibrils. The sample collection and preparation for TEM analysis are highly complex, and the accuracy of measurements can be skewed by biases. Therefore, inaccurate measurements can arise from non-uniform fiber deposition resulting from inertial, gravitational, and electrostatic forces, as TEM analysis examines only small portions of the filter. Additionally, fibers that penetrate the filter surface without being successfully transferred to the carbon film may be lost. However, incomplete dissolution of the filter can hinder analysis. Many of the biases and variability observed in fiber sampling and counting using PCM also apply to TEM. Furthermore, fiber counting in TEM can introduce additional inconsistencies, as the high magnification often leads to an emphasis on detecting the smallest fibers while overlooking larger ones. Despite this, fibers shorter than 0.5 µm are frequently undetected due to their low visibility against background noise in the sample. (Baron 2001)

4.5 Direct reading fiber measurement

Direct-reading monitors may also be utilized in laboratory studies where fibers are the primary component in the aerosol. To enable more precise measurement of fibers in the presence of compact particles, a fibrous aerosol monitor was constructed. This instrument identifies fibers through a combination of electrostatic alignment and optical scattering techniques. A commercial version, the Fibrous Aerosol Monitor (FAM), was later introduced. An investigation into fiber length measurement using light scattering in the FAM demonstrated a strong correlation between fiber lengths obtained through this method and those measured via SEM analysis. Additionally, other direct-reading instruments that integrate fiber alignment and light scattering have been designed for asbestos monitoring. Rood et al. developed a method in which fiber alignment occurs through shear forces in an inlet tube, followed by electrostatic precipitation for deposition and differential light scattering for detection. (Rood et al. 1992) A different appliance, the Fibrecheck™, distinguishes between fibers and compact particles by analyzing scattering at multiple angles. (Kulkarni 2011)

4.6 Measurement of concentration

Measurement of concentration and qualitative analysis of fibers were executed by Li et al. (2020). The study described the composition and shape of fibers captured either on the roof of the building of the campus of a university or at the human respiratory height of 1,5 m above the ground. Suspended particles were collected on mixed cellulose ester. The samples were prepared and analyzed by scanning electron microscopy method for the determination of the number concentration of fiber particles in ambient air. An EDX attached to the SEM was used to obtain the composition of elements. Randomly chosen 50–100 fields of view were applied for the counting. The elemental composition of fiber particles identified with EDX was used to determine the preliminary fiber type. In addition, the number concentration of the fiber particles in the air was estimated using Equations (4) and (5) (Li et al. 2020):

$$C_i = \frac{n_i}{N * V_B} \tag{4}$$

$$V_B = \frac{4 * F_B * V}{\pi * d_{eff}^2} \tag{5}$$

where: Ci is the concentration of fiber type i, n_i is the number of fibers counted for fiber type i, N is the number of image fields examined, V_B is the sampled air volume per field, F_B is the area of the image field, V is the total sampled air volume, d_{eff} is the effective filter diameter. (Li et al. 2020)

Fiber particles were categorized into two primary groups: organic fibers and inorganic fibers, based on their morphology, stability under the electron beam, and elemental composition. Organic fiber particles include both microplastic and naturally occurring organic fibers. On the other hand, a group of inorganic fibers contains man-made mineral fibers (MMMFs), asbestos, calcium sulfate, and metal fiber particles. Li et al. (2020) presented that fibers of various compositions are often accompanied by small attached particles, as seen in Figure 11. (Li et al. 2020)

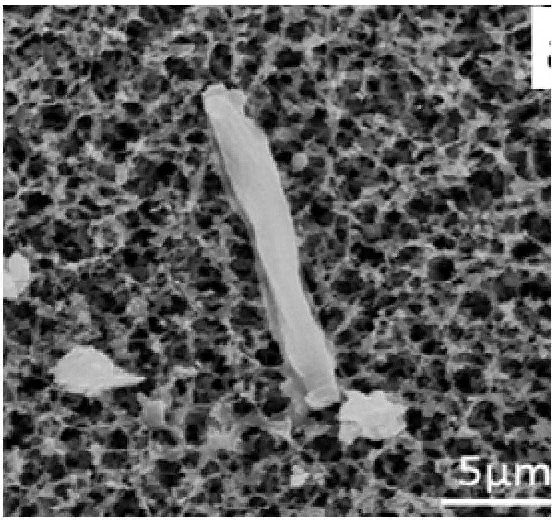

Figure 11 Microplastic fiber (Li et al 2020)

Microplastic fibers, natural organic fibers, calcium sulfate, and MMMFs all appeared as regular fibers, with slight variations for natural organic fibers, which were elongated and their structure was not uniform, and MMMFs, which had a bar-like structure. Asbestos fibers had a distinct fibrous and needle-like structure with smooth surfaces. However, metal fibers varied in shape, appearing as both regular and irregular fibers. The chemical composition of the fibers was mainly carbon and oxygen for microplastic and natural organic fibers; MMMFs were predominantly composed of silicon and oxygen. Nevertheless, some fibers displayed a complex composition of silicon, magnesium, aluminium, and potassium, suggesting that they were mixtures of fibers and minerals. Asbestos was prominent in silicon and magnesium. The composition of metal fibers was iron, titanium, magnesium, and sodium. (Li et al. 2020) Microplastic fibers exhibited a regular fibrous structure with smooth surfaces and were easily identifiable under high-resolution SEM. Their primary elemental components were carbon and oxygen, with some fibers also containing minor amounts of sodium, magnesium, aluminum, silicon, potassium, and calcium. (Li et al. 2020)

The relative percentages of fiber particles in the air differed at the measured sites: the roof of the building (RB) and the human respiratory height (HRH), although fiber particles exhibited similar types and length ranges. At the RB site, fiber particle lengths ranged from 5 µm to 200 µm, with approximately 80% falling within the 5–20 µm range. Similarly, at the HRH site, 84% of the fiber particles were within this length range. Comparing the types of fiber particles present in surface dust are similar to those found in airborne particles, the fibers in surface dust tend to be larger. This finding suggests that 20 µm may be the critical threshold for fibers to remain suspended in the air, with larger fibers settling more quickly and not staying airborne for extended periods. Microplastics constituted 41.3% of the fiber particles at the RB site and 34.6% at the HRH site. This discrepancy may be due to the lower density of microplastic fibers, which makes them more easily suspended in the air compared to other fiber types of similar size. Bergmann et. al (2019) suggest that microplastics, both granular and fibrous, can be transported through the atmosphere and ocean currents to virtually any location on Earth, including remote regions such as the Arctic (Bergmann et. al, 2019). The proportion of MMMF particles at the HRH sampling site was approximately 10% higher than at the RB site. Unlike microplastic fibers, MMMF particles are denser and therefore less likely to remain suspended in the air. Consequently, MMMFs tend to accumulate in the near-surface atmosphere. The percentages of asbestos and calcium sulfate fiber particles at the RB and HRH sites were comparable, around 7,5% for both types at both sites, suggesting an even distribution of these fibers in the air. Both asbestos and calcium sulfate occur naturally in fibrous forms and can be mechanically fragmented into finer fibers by external forces, increasing their ability to remain airborne. At the HRH sampling site, metal fiber particles made up 5.6% of the total, nearly double the 2.3% observed at the RB site. Their higher density makes them less prone to resuspension into the upper atmosphere, leading to their greater concentration near the ground. Consequently, metal fiber particles have a restricted ability to disperse over long distances. (Li et al. 2020)

Evans, Ki (2010) monitored aerosol concentration in a facility producing CNFs. In occupational settings involving the manufacture, processing, or handling of nanomaterials, there remains a lack of consensus regarding the most appropriate particle exposure metrics to monitor. It has been recommended that, at a minimum, particle number concentration, surface area, and mass should be concurrently assessed to effectively evaluate nanomaterial exposure. However, in practice, workplace assessments that incorporate multiple metrics are generally constrained to area or static sampling methods. In manufacturing environments, industrial processes frequently generate signature aerosols distinguished by specific particle size distributions and/or unique chemical composition. Conducting detailed aerosol size characterization can enhance the understanding of contaminant transport mechanisms and the potential for inhalation exposure. Among the various metrics assessed, particle mass was identified as the most practical and effective for monitoring CNF emissions. The use of a photometer in direct-reading applications provided a reasonable estimation of respirable CNF mass concentration. Furthermore, chemical analysis techniques enabled the selective identification of CNFs amidst other airborne workplace contaminants. Particle size distribution was characterized using both an electrical low-pressure impactor and a fast particle size spectrometer. Collectively, the concurrent monitoring of multiple metrics proved valuable in distinguishing emission sources and quantifying the relative contributions of different airborne particles within the occupational environment. (Evans, Ki 2010)

5 Classification methods for fibrous aerosols

The classification of fiber-like particles by size is inherently challenging, as it requires simultaneous consideration of both fiber diameter and length during the separation process. To date, no single separation mechanism has proven capable of effectively distinguishing fibers based on these two-dimensional attributes simultaneously. (Baron 2001)

5.1 Fiber separation by diameter

The aerodynamic diameter of fibers is mainly determined by their physical diameter and density, with fiber length having a slight influence. Hence, the aerodynamic diameter compares the settling behavior of distinct shapes and densities and homogenizes the shape and density of particles. Fiber separation by diameter has been utilized by various systems, like cyclones, impactors, and porous foam classifiers. It was shown that fibers with larger diameters enable exponential decrease of average fiber concentration in workplaces, demonstrating the faster settling of fibers with larger diameters. (Baron 2001)

Aerosol centrifuges are widely used to separate particles and fibers by size. The operation of these devices relies on a combination of centrifugal and Coriolis forces, which drive particle deposition along the outer walls of a spinning duct. The basic working principle of a centrifuge consists of purified sheath air that enters through a flow-stabilizing laminator and traverses the rotating duct under high-speed centrifugation. The polydisperse aerosol sample is introduced via a slit adjacent to the inner wall, and are transveresed though the spiral duct. Under fixed operational parameters, deposition position along the outer wall is predominantly determined by particle size. Larger-diameter particles experience greater centrifugal forces, depositing first, while smaller particles remain entrained in the flow for longer transport distances. Sufficient centrifuge length ensures total particle deposition. (Asgharian 1999)

5.2 Dielectrophoresis

Dielectrophoresis (DEP) is described as the motion of neutral particles under the influence of a nonuniform electric field. The dielectrophoretic force is governed by particle volume, geometry, and material properties, enabling charge-neutral particle separation without requiring net surface charge. (Pesch, Du 2021)

The mechanism of dielectrophoresis can be described as follows. A neutral particle will polarize in an electric field. Charge separation within the particle generates charges of equal magnitude and opposite signs on its opposing sides of the particle. The charges are subjected to Coulomb forces induced by the electric field. In the presence of a uniform electric field, these forces would cancel out due to the equal magnitude of the charges. However, when the field is nonuniform, the force exerted on one side of the particle is slightly weaker, resulting in a net force. The suspended particle experiences dielectrophoretic motion as the result of the net force formed by the nonuniformity of the field. The motion is governed by the applied alternating current. In an AC electric field, the polarity of all charges reverses every half-cycle, yet the consequent interactions and forces remain consistent due to the symmetric nature of the field oscillations. The use of AC voltage has the advantage that movement is only caused by dielectrophoresis and does not interfere with electrophoretic phenomena. (Iglesias, Santamaría, López, Domínguez 1989); (Pesch, Du 2021)

The effect of the electric field is not only applied to the particle but also to the surrounding suspension, which results in a polarization of both the particle and the suspension. Accumulation of polarization charges is present on the surface of the particle, in the particle itself, and also in the surrounding medium. This process is referred to as Maxwell–Wagner interfacial polarization. The interfacial charge distribution exhibits polarity, with counterions accumulating on each side. The polarization of a material depends on the permittivity of said material. Consequently, the amount of charges inside and outside of the particle may vary, as it is the direct result of the permittivity of the material. The particle experiences negative polarization when the charge outside of the particle is larger, while the particle is less polarizable. Negative polarization, also known as nDEP, sets the particle in motion against the field gradient, away from the local field maxima. Alternatively, if the charge is greater inside the particle than outside, the particle experiences positive polarization pDEP and moves toward the local field maxima, as illustrated in Figure 12. The total polarization arises from two distinct mechanisms: a dielectric component resulting from the displacement of charges from their equilibrium positions, and a conduction component associated with mobile charge carriers. (Pesch, Du 2021)

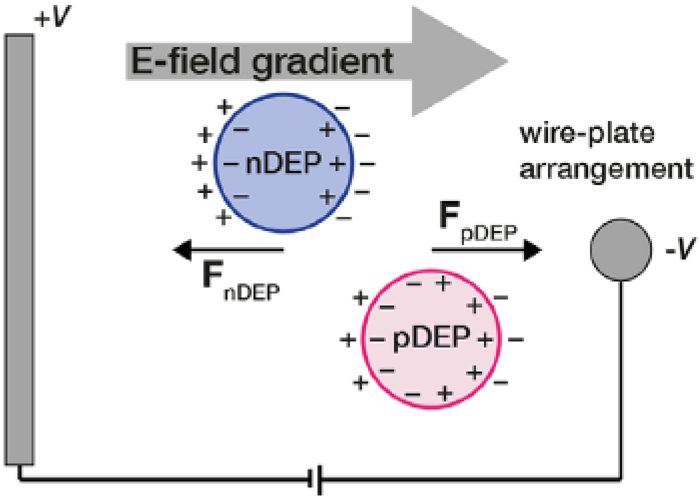

Figure 12: Particle polarization in a nonuniform field (Pesch, Du 2021)

Moreover, the polarization of particles induces attractive forces on the neighboring particles, causing the particles to interact and interfere with each other. The phenomenon is known as mutual dielectrophoresis. This results in alignment into pearl chain formation oriented either parallel or perpendicular to the electrical field. Chain formation can prevent the successful separation of individual particles, due to the overpowering properties of the chains. Target and non-target particles are engulfed in the chains, and the separation efficiency is largely influenced. Particle concentration has an impact on the separation efficiency due to increased interaction between the particles, as the distance between particles is reduced. To prevent dipole-dipole interaction between particles, an average particle spacing of three particle diameters must be ensured, as expressed by Gascoyne, Shim (2014). (Iglesias, Santamaría, López, Domínguez 1989); (Gascoyne, Shim 2014)

Electrode geometries and different configurations are crucial in the results of dielectrophoresis, as they significantly affect the nonuniformity of the field. The most common layout of the electrodes is spherical, cylindrical, and isomotive. Spherical and cylindrical configurations result in a more intense nonuniform electrical field and are beneficial for different aims of the investigation. Non-spherical particles can be reoriented with respect to the lines of the electric field. (Iglesias, Santamaría, López, Domínguez 1989)

For a particle in an AC electric field with amplitude E, the time-averaged DEP force can be expressed as:

$$F_{DEP} = \pi\epsilon_m\epsilon_0 a^3[K_{CM}]\nabla|E|^2 \quad (6)$$

Where, ϵ_m is the relative permittivity of the medium, ϵ_0 is the vacuum permittivity ($\epsilon_0 = 8.854\cdot10^{-12}$), K_{CM} is the Clausius-Mossotti factor, describing the particle's relative polarizability in the medium and determines the movement direction of the particle in the field, a is the radius of a homogenous spherical particle, E is the amplitude of the AC electric field. (Pesch, Du 2021)

Even though equation (6) predicts nDEP almost independently of the frequency, various particles would show pDEP, relying on the suspension conductivity. This irregularity is seen in non-conductive particles such as silica or polystyrene, and is attributed to the double layer enhancing the overall conductivity of the particles. (Pesch, Du 2021)

Baron, Deye, and Fernback (1994) developed an instrument for the classification of fibers according to their length using dielectrophoresis. The classifier, Figure 13, is composed of two concentric cylinders, where in the annular region between the cylinders, the classification occurs. Fibrous aerosol is introduced at the top of the classifier, while sheath flow is at the bottom. The airflow through the annular region is laminar (Re = 100). The fibers are attracted by the dielectrophoretic force to the inner cylinder as a result of the high-voltage field application to the system. The original design was set up to capture the fibers on the inner electrode, as it was coated with oil. The fibers were classified according to their different dielectrophoretic mobilities, which were influenced by their length and caused the fibers to move with different velocities towards the inner electrode. (Baron, Deye, Fernback 1994)

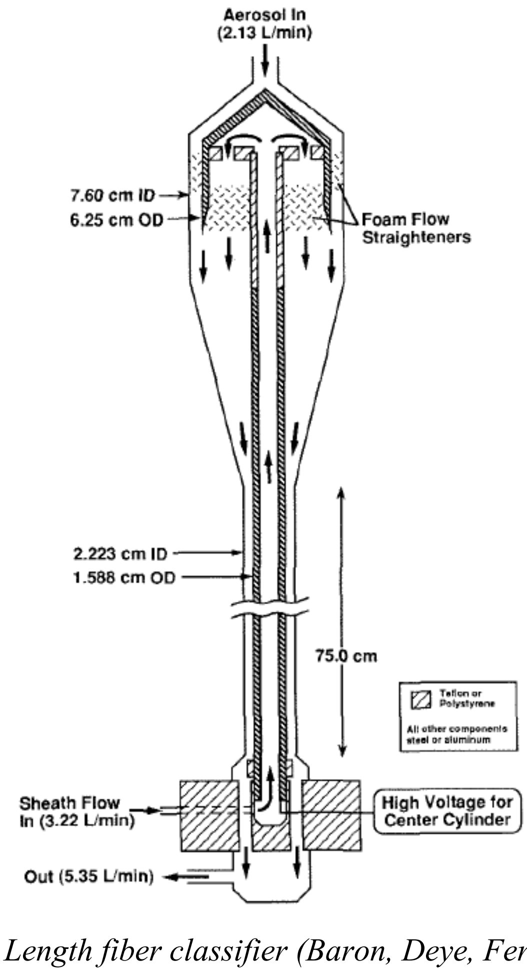

Figure 13: Length fiber classifier (Baron, Deye, Fernback 1994)

The development of the classifier by Baron, Deye, Fernback (1994) was inspired by earlier work of Lipowicz, Yeh (1989), who explored the idea of fiber length separation with the utilization of dielectrophoresis. The research revealed that dielectrophoretic forces could effectively separate aluminum wires ranging from 0.5 to 5 mm in length as they settled through a liquid medium. The results established that a fiber length classifier could be developed using dielectrophoresis principles. (Lipowicz, Yeh 1989)

Baron, Deye, Fernback (1994) successfully classified fibers based on their length. The lengths of asbestos fibers varied from 8 to 31µm. They also stated that the classifier efficienly removed fibers longer than 16 µm, and could serve as low pass filter and produce aerosols with short fibers only.(Baron, Deye, Fernback 1994)

Wang et al. (2005) studied the additional utilization of the classifier developed by Baron, Deye, Fernback (1994) and focused on the influence of humidity of the carrier air on classification process, as they classified carbon fibers which are conductive and glass fibers which are non-conductive. The classification of carbon fibers was not affected by the changes of the average air humidity. However, glass fibers became classifiable when the relative humidity exceeded 15%. (Wang et al. 2005)

Deye et al. (1999) analysed the flow field of the classifier using computational fluid dynamics and identified flow disturbances in the original design, particularly in the inlet and outlet regions that could degrade resolution. They addressed these issues through design modifications. Additionally, the study examined the effect of the airflow ratio on classification. It was found that balancing the ratio of airflows influences the length distribution, reducing the sheath flows decreases the minimum classifiable length, but broadens the overall length distribution. (Deye, Gao, Baron, Fernback 1999)

5.2.1 Mathematical formulation of dielectrophoric force

Lipowicz, Yeh (1989) derived an equation for the time of motion between the initial and final radius. The equation is based on a prolate spheroid placed in a vacuum where the dielectrophoretic force exerts force in the spheroid, whose dimensions are comparatively small to the dimensions of the field. For a fiber that is simplified into a form of prolate spheroid with length *L* and with diameter *D,* the dielectric force (7) caused by a nonhomogeneous electric field is given by:

$$F = \frac{\pi K_m \epsilon_0}{12} D^2 L \left[\frac{\alpha}{\alpha - 1} - f(\beta)\right]^{-1} \nabla E^2 \tag{7}$$

where K_m is the dielectric constant of an electrically insulating medium (K_m = 1.00058986 for air), ϵ_0 is the permittivity of vacuum (ϵ_0 = 8.85418782·10^{-12} F/m), η is the dynamic viscosity (η = 0.00001516 m2/s, for air), $\alpha = K_f/K_m$ is the ratio between the dielectric constant the fiber and of the insulating medium, *E* is the electric field. And the function of fibrocity $f(\beta)$ is given by:

$$f(\beta) = \frac{\beta}{\sqrt{(\beta^2 - 1)}}\left[\left(1 - \left(\frac{\beta}{\sqrt{(\beta^2 - 1)}}\right)^2\right) \cdot coth^{-1}\left(\frac{\beta}{\sqrt{(\beta^2 - 1)}}\right) + \frac{\beta}{\sqrt{(\beta^2 - 1)}}\right] \tag{8}$$

where β is the aspect ratio of the fiber.

The drag force F_D on a prolate spheroid moving in a viscous fluid, when the motion is parallel to the major axis, is given by:

$$F_D = 3\pi D v g(\beta) \tag{9}$$

where v is the deposition velocity and $g(\beta)$ is a function of the fibrocity given by:

$$g(\beta) = \frac{8}{3}\left[\frac{-2\beta}{\beta^2-1} + \frac{2\beta^2-1}{(\beta^2-1)^{3/2}}\, ln\frac{\beta+(\beta^2-1)^{1/2}}{\beta-(\beta^2-1)^{1/2}}\right]^{-1} \tag{10}$$

Velocity of the fiber in the classificator stems from equating the dielectrophoretic (7) and drag force (9):

$$v = \frac{K_m\epsilon_0}{36\eta} DL\left\{g(\beta)\left[\frac{\alpha}{\alpha-1} - f(\beta)\right]\right\}^{-1} \nabla E^2 \tag{11}$$

The velocity seems to be linearly dependent on length, however, the effect of the fibrocity functions $g(\beta)$ and $f(\beta)$ has to also be factored in. Suppose that the fibers would the significantly longer than the diameter, so $\beta \Rightarrow \infty, f(\beta) \Rightarrow 1$, meaning that the function g(β) becomes:

$$g(\beta) =_{lim\,\beta=>\infty} \frac{2\beta}{3(ln2\beta - 0{,}5)} \tag{12}$$

Supposing that the fiber is conductive $K_f=\infty$, $\frac{\alpha}{\alpha-1} = 1$, and infinitely long $\beta \Rightarrow \infty$, the dielectric velocity is given by:

$$v = \frac{K_m\epsilon_0}{24\eta} L^2 \frac{(ln2\beta - 0{,}5)}{(ln2\beta - 1)} \nabla E^2 \tag{13}$$

Under the condition that $\beta > 5$, Equation (13) is comparable to Equation (11) without any significant deviation (Lipowicz, Yeh 1989).
The electric field between infinite concentric cylinders may be written in the general form:

$$E = \frac{cU}{r} \tag{14}$$

where U is the applied voltage, r is the radial distance, and c is a constant dependent on the electrode size and spacing and insulation thickness and material. Implementing Equation (14) into Equation (13) and subsequent mathematical operations (15), (16), (17), (18) yields the time required for the particle to move from an outer radius R_{out} to an inner radius R_{in}. Where the square of the electric field is derived in cylindrical coordinates (15), subsequent implemenation into Equation (13), and separation of variables (17), integration (18), and the final solution for time of deposition (19).

$$\nabla E^2 = \left[\frac{\partial E^2}{\partial r}, \frac{1}{r}\frac{\partial E^2}{\partial \varphi}, \frac{\partial E^2}{\partial z}\right] = \left[\frac{\partial\left(\frac{cU}{r}\right)^2}{\partial r}, \frac{1}{r}\frac{\partial\left(\frac{cU}{r}\right)^2}{\partial \varphi}, \frac{\partial\left(\frac{cU}{r}\right)^2}{\partial z}\right] = \left[\frac{-2c^2U^2}{r^3}, 0{,}0\right] \tag{15}$$

$$\frac{dr}{dt} = \frac{K_m\epsilon_0}{24\eta} L^2 \frac{(ln2\beta - 0{,}5)}{(ln2\beta - 1)}\left[\frac{-2cU}{r^3}, 0{,}0\right] \tag{16}$$

$$\int_{r_1}^{r_2} -r^3 dr = \int_0^t \frac{K_m \epsilon_0}{24\eta} L^2 \frac{(ln2\beta - 0{,}5)}{(ln2\beta - 1)} [2c^2V^2, 0{,}0]\, dt \tag{17}$$

$$\frac{1}{4}(R_{out}^4 - R_{in}^4) = \frac{K_m \epsilon_0 c^2 U^2}{12\eta} L^2 \frac{(ln2\beta - 0{,}5)}{(ln2\beta - 1)} t \tag{18}$$

$$t = \frac{3\eta(R_{out}^4 - R_{in}^4)}{K_m \epsilon_0 c^2 U^2 L^2} \frac{(ln2\beta - 1)}{(ln2\beta - 0{,}5)} \tag{19}$$

The Equation (19) is described by Lipowicz, Yeh (1989), the depositon time is not affected by the frequency of the AC field.

Baron, Deye, Fernback (1994) enhanced the formulas (11) and (19) originally derived by Lipowicz, Yeh (1989), where the main improvement was the implementation of the formulas for the electric field forming Equation (20):

$$t = \left(\frac{360000}{1{,}5} \frac{\eta}{K_m \epsilon_0 U^2} \left[ln\left(\frac{R_{out}}{R_{in}}\right)\right]^2\right) \frac{r_0^4 - r^4}{DL} g(\beta) \left(\frac{\alpha}{\alpha - 1} - f(\beta)\right)$$

Pankrác (2020) states the intensity of the electric field between two axially aligned cylinders as written in Equation (21):

$$E(r) = \frac{\tau}{2\pi\epsilon_0} \frac{1}{r} \tag{21}$$

where E is the intensity of the electric field, τ is the linear charge, ϵ_0 is the permittivity of vacuum, r is the radial distance between the cylinders. The voltage can be described as:

$$U = \int_{Rin}^{Rout} E(r)\, dr \tag{22}$$

where R_{out} and R_{in} are the radii of the outer and inner electrodes, respectively. Substitution of equation (21) into (22) yields:

$$U = \int_{Rin}^{Rout} E(r)\, dr = \frac{\tau}{2\pi\epsilon_0} \int_{Rin}^{Rout} \frac{1}{r} dr = \frac{\tau}{2\pi\epsilon_0} \ln\left(\frac{R_{out}}{R_{in}}\right) \tag{23}$$

where it describes the relation between the linear charge that is created between the cylinders, after the voltage is applied. Expressing the linear charge from Equation (23)

$$\tau = \frac{2\pi\epsilon_0\, U}{ln\left(\frac{R_{out}}{R_{in}}\right)} \tag{24}$$

Substituting Equation (24) into (21). The following can be derived:

$$E = \frac{\tau}{2\pi\epsilon_0}\frac{1}{r} = \frac{2\pi\epsilon_0}{\ln\left(\frac{R_{out}}{R_{in}}\right)}U\frac{1}{2\pi\epsilon_0}\frac{1}{r} = \frac{U}{\ln\left(\frac{R_{out}}{R_{in}}\right)r} \tag{25}$$

This indicates that the electric field intensity is influenced exclusively by the applied voltage and the interelectrode distance, attaining its maximal magnitude at the surface of the inner cylindrical electrode. (Pankrác 2020)

Equation (25) establishes the groundwork for subsequent derivations, including the time necessary for fiber classification. The following are the partial calculations and substitution in Equation (11). Equation (26) represents the derivation in cylindrical coordinates of the square of the electric field:

$$\nabla E^2 = \frac{\partial}{\partial r}\left(\frac{U}{\ln\left(\frac{R_{out}}{R_{in}}\right)r}\right)^2 = \frac{U^2}{\left(\ln\left(\frac{R_{out}}{R_{in}}\right)\right)^2}\frac{-2}{r^3} \tag{26}$$

The following equation displays the substituted Equation (26) into (11):

$$\frac{dr}{dt} = v = \frac{K_m\epsilon_0}{36\eta}DL\left\{g(\beta)\left(\frac{\alpha}{\alpha-1} - f(\beta)\right)\right\}^{-1}\frac{U^2}{\left(\ln\left(\frac{R_{out}}{R_{in}}\right)\right)^2}\frac{-2}{r^3} \tag{27}$$

Separation of variables (28) and subsequent integration (29) is the necessary next step to achieve the relation (30) of deposition time to the other variables.

$$\int_{r_0}^{r} -r^3 dr = \int_0^t \frac{K_m\epsilon_0}{36\eta}DL\left\{g(\beta)\left(\frac{\alpha}{\alpha-1} - f(\beta)\right)\right\}^{-1}\frac{2U^2}{\left(\ln\left(\frac{R_{out}}{R_{in}}\right)\right)^2}dt \tag{28}$$

$$\frac{1}{4}(r_0^4 - r^4) = \frac{K_m\epsilon_0}{36\eta}DL\left\{g(\beta)\left(\frac{\alpha}{\alpha-1} - f(\beta)\right)\right\}^{-1}\frac{2U^2}{\left(\ln\left(\frac{R_{out}}{R_{in}}\right)\right)^2}t \tag{29}$$

$$t = \frac{4{,}5\eta}{K_m\epsilon_0 U^2}\frac{r_0^4 - r^4}{DL}g(\beta)\left(\frac{\alpha}{\alpha-1} - f(\beta)\right)\left[ln\left(\frac{R_{out}}{R_{in}}\right)\right]^2 \tag{30}$$

Equation (30) represents the time of motion between the initial and final radius of the cylindrical electrodes. The equation derived here (30) and the equation (20) presented by Baron, Deye, Fernback (1994) and equation (19) by Lipowicz, Yeh (1989) differs in the scalar multiple, as in the equation (20) there is present scalar multiple of 240000 to match the experimental results and units used by Baron, Deye, Fernback (1994), while the time of depostion (19) is divided by 2,4 in the study by Lipowicz, Yeh (1989), to also match the experimental results. (Baron, Deye, Fernback 1994); (Lipowicz, Yeh 1989)

5.3 Electrophoresis

Electrophoresis refers to the movement of charged aerosol particles within an electric field. Electrostatic forces have been successfully employed for the control of submicron-sized particles. Both theoretical analyses and experimental investigations have demonstrated that, under electrostatic separation, the electric mobility of a fiber is approximately 1,8 times greater than that of a sphere with an equivalent aerodynamic diameter. The electric charge acquired by particles is influenced by several factors, including particle size and morphology, ion concentration, the strength of the applied electric field, and the residence time within the charging zone. It was shown, through calculations and subsequent experimental validation, that fiber separation based on length can be achieved by introducing aerosol samples into a unipolar charging region, followed by passage through an electrostatic precipitator. Long, slender fibers exhibited a higher rate of charge acquisition compared to more compact particles, and the resulting differences in electric mobility were utilized to facilitate separation by length. (Han, Moss, Wong 1994)

Under unipolar diffusion charging conditions, the number of charges acquired by fibers of identical diameter is directly proportional to their lengths. Length becomes the primary determinant in electrophoretic separation for fibers with uniform diameter, largely independent of their electrical conductivity. (Han, Moss, Wong 1994)

Aerosols are classified by electrophoresis according to their electrical mobilities, which, for a fiber, are determined by the charge number and are inversely proportional to the product of diameter and shape factor. Since the shape factor is generally only weakly dependent on fiber length, and the charge number is proportional to fiber length, electrophoretic separation is more effective for fibers with a diameter in similar size range. Hence, prior to electrophoretic separation, fibrous samples should be subjected to aerodynamic separation to achieve an initial diameter-based separation. Although dielectrophoresis is proven to be more effective than electrophoresis for longer fibers to execute length-based separation, electrostatic precipitation proves more practical for fibers with lengths below 5 µm and diameters under 1 µm. In the case of conductive samples, dielectrophoretic separation offers the advantage of enabling the preliminary removal of particulate contaminants. Subsequently, diameter-based fiber separation must be accomplished through aerodynamic classification. (Han, Moss, Wong 1994)

5.3.1 Size classification of carbon fibers by an electrical method

An electrical method can be utilized to classify, as demonstrated by Chen et al. (1993). The number of charges on the fibers is largely determined by their length. The differences in electrical mobility facilitate the classification by length. In the study, amorphous carbon particles were subjected to the classification process. The bulk material had to undergo treatment in the form of milling to create particles that could be airborne. The milled product consisted of fibers with identical diameters but varied in length and some non-fibrous debris. To filter out the non-fibrous particles, a method of filtering through a three-stage cyclone was implemented five times. Cyclone-classified material was used to generate airborne fibers using a small-scale powder disperser. To achieve a state of Boltzmann charge equilibrium, the aerosol was subsequently passed through an ^{85}Kr bipolar ion source. A modified electrical aerosol analyzer was utilized for the classification of fibers according to their length. Following exposure to positive ions, the aerosol particles became electrically charged. The amount of positive charge, produced by high voltage, acquired by a fiber-like particle, was determined by its diameter and length and was influenced by the ion concentration, the residence time of the particle in the charging region. The aerosol flow was introduced into an electric mobility precipitator, which consisted of a space between two concentric cylinders, where the inner cylinder was charged with a negative high voltage. The deposited particles were captured on a thin layer of Mylar segments. To ensure the visibility of every fiber, the segments were treated with ethanol, which caused the rotation of fibers to a parallel position to the surface of the segments. It was shown that the carbon fibers can be classified by length in the presence of a positive electric charge and passing through the electric mobility precipitator. It is suggested that to implement this length classifying process for fiber particles in an environmental setting, which are smaller and vary in diameter and length, that two-step procedure would be necessary. Firstly, to sort fibers by diameter and then to apply the electrical method to distinguish them based on length. (Chen, Yeh, Hobbs 1993)

5.4 Dustiness

However, the production and handling of CNTs and CNFs increase potential health hazards linked with occupational exposure. Ku and Birch (2019) observed the dustiness of nanomaterials and concluded that the relationship between dustiness and bulk dustiness is generally strong for fibrous nanomaterials but may be comparatively weaker for fine and coarse materials lacking fibrous structure. The bulk density of a powder is defined as the ratio of the mass of an untapped powder sample and its volume, including the contribution of the inter-particulate void volume (Ku, Birch 2019). Dustiness is the tendency of a bulk nanomaterial to become airborne. Dustiness may be defined as the propensity of a powder to form airborne dust by a prescribed mechanical stimulus (Evans, Turkevich 2012). CNT powders with lower bulk density and looser agglomeration are more prone to dispersion, particles remain airborne for longer periods. Given the particle size, these materials can present elevated exposure risks due to their high dispersibility and prolonged suspension in the air. (Ku, Birch 2019)

An acoustic-based fluidized bed generator was employed to aerosolize carbon CNTs and CNFs. The study encompassed SWCNTs, MWCNTs, and CNFs with outer diameters ranging from 1.01 nm to 100 nm and lengths spanning 1.02 μm to 100 μm. (Ku, Birch 2019)

Aerodynamic diameter increased with bulk density, whereas mobility diameter decreased, reflecting structural compactness. SEM images confirmed less agglomerated, fibrous structures in low-density materials versus compact morphologies in high-density ones. Low bulk density CNTs pose higher inhalation risks due to prolonged airborne residence and ease of dispersion. Bulk density is a critical predictor of aerosolization potential and exposure risk for CNTs/CNFs. Loosely agglomerated, low-density materials disperse more readily and remain airborne longer, necessitating stringent controls in occupational settings. The study underscores the need for material-specific risk assessments and supports using bulk density as a practical metric for exposure evaluation (Ku, Birch 2019)

5.5 Wire mesh filtration

Myojo (1999) created a method for determining the length distribution of fibrous aerosol. The process consisted of the simulation of fiber collection on a wire mesh and subsequent comparison with experimental results for three types of fibers. The fibers during the simulation are assumed to have a small diameter so that the only sedimentation process is interception, and the wire mesh screen was always simulated as empty, so that the already collected fibers did not affect the process. The experimental method utilized glass fibers and four different wire mesh screens. The meshes were situated 5 mm apart so that the spacing between the mesh layers significantly exceeds the fiber dimensions, and the filtration process at each mesh can be considered independent. The fibers were collected on filters and counted by SEM. Experimental validation with glass fiber aerosols supported the simulation results of penetration through wire mesh screens, particularly for fibers with a large fiber length to mesh opening ratio. The dominant collection mechanism was interception, not inertia, as confirmed by low collection efficiency for compact particles. Thus, wire mesh screens selectively captured fibers while allowing most spherical particles to pass through. (Myojo 1999)

6 Methodology of classification of fibrous aerosols

The thesis aimed to execute a classification of fibrous aerosols based on the length of the fibers. The experiment was based on the previous measurments done by Baron, Deye, Fernback (1994) and Wang et al. (2005). The goal was to compare the quality of classification depending on various input parameters, such as varying humidity of the carrier gas, creating various electric fields by changing the applied voltage, and experimenting with the amount of the airflows.

6.1 Glass fiber preparation

To ensure workplace health and safety, the process must be done while wearing a respirator and protective gloves. Preparation of the mixture of glass fibers and glass beads is the first step in the process of the experiment. Glass fibers used in the experiment were obtained by milling glass-blowing insulation Supafil® Loft (Knauf Insulation GmbH). A glass insulation sample of 1,3 g was pressed three times with a pressure of 7000 kp for 30 seconds, which produced clumps of glass fibers. After each press, the sample was mixed and loosened from the bottom of the press to guarantee optimal comminution. Subsequently, the clumps of glass fibers were mixed with Ballotini impact glass beads (Potters Industries Inc.) in a weight ratio of 2% to 98%, respectively. To achieve homogeneous consistency, sifting the mixture of the glass fibers and glass beads was repeated four times through sieves with decreasing mesh width (840 μm, 425 μm, and 420 μm).

6.2 Experimental system

The mixture of glass fibers and glass beads was transferred to a hopper for a primary stock and subsequent processing. A rotary feeder continually dispensed the mixture further. Figure 14a displays the hopper connected to the rotary feeder. The hopper was covered to prevent resuspension of the fibers into the laboratory. The rotary feeder is composed of a DC electrical motor from which the shaft with a rotational wheel made from Plexiglas. The circumference of the impeller is covered with a velcro strip. Rotation settings were adjusted from the initial setting of 3 to 0,9 on a potentiometer, which regulates the rotational speed of the motor, as a result of the exchange of the velcro type on the propeller, as it became saturated with glass fibers during the duration of the experiment.

The airflow from the laboratory distribution system was humidified to different levels according to a particular measurement necessity. The humidifying setup used was the same as in the study by Lizal et al. (2019), with a few changes. The humidification occurs in a sealed box, where a single inlet is connected to the laboratory distribution system and an outlet on the other side discharges the humidified air. The humidification of the airflow as it passes through the box occurs just from the water surface. The desired humidity level is achieved by mixing the humidified air with a bypass of an airflow with low humidity. The humidity level is controlled by a sensor placed downstream after the mixing has occurred. The humidified airflow is divided into three airflows with controlled flows. Two sheath flows, S1 and S2, which served to eliminate fiber deposition on the walls of the classifier, and one aerosol flow, AER_IN, which contained the fibrous aerosol. There were two airflows leaving the classifier: Q_C, which was the flow of the classified fibers, and Q_D, which was the dump flow with all the fibers of undesired length.

The mixture of glass fibers and glass beads is mixed with pressurized air from the laboratory's distribution system and afterwards fed into a high–speed orbital shaker, Wisd VM 10 (Witeg Labortechnik GmbH). The shaker, which can be seen in Figure 14b, performs orbital motion with adjustable settings from 0 to 3300 rpm. The shaker was configured to operate at approximately 2/3 of its maximum capacity, corresponding to setting 9 out of a possible 13 levels. The vibrational motion of the shaker generates a boundary layer, where the suspension of fibrous particles is achieved, meaning that the formation of fibrous aerosol is created. Consequently, the heavier glass beads are separated from the mixture and collected into a collecting beaker. This process resulted in the formation of a fibrous aerosol. On the other hand, the fibers are transported by the AER_IN airflow.

Figure 14: a) Rotary feeder and hopper, b) orbital shaker

The static electrical charge from the fibers was removed by the neutralizer NEKR-10 (Eckert a Ziegler CESIO), which contains ^{85}Kr.

The aerosol flow AER_IN enters the classifier at the top and also does the sheath flow S1; on the contrary, the sheath flow S2 enters at the bottom of the classifier and rises through the middle electrode to the top.

The classifier is configured with two concentric tubular electrodes, where the strongest electric field is present at the surface of the inner electrode. To help minimize the risk of turbulence, a smooth, low-angle conical transition section was incorporated at the top of the classifier where the flows encounter. The classification occurs within the annular region between the two concentric cylinders, spanning a length of 75 cm. The inner cylinder has an outer diameter of 1.59 cm, and the outer cylinder has an inner diameter of 2.22 cm. The aerosol sample is injected between coaxial sheath flows within an annular electrode configuration. Application of high voltage across the electrodes creates a gradient electric field, inducing dielectrophoretic forces that selectively affect fibers within a defined length range. The system outputs two streams: a classified flow containing fibers of desired length and a dump flow carrying other particles. To mitigate high-voltage discharge phenomena, all metallic surfaces were coated with a mixture of grease and immersion oil to prevent particle resuspension.

The electrical conductivity of fibers is a crucial condition for a successful dielectrophoretic classification of fibers. While glass fibers are inherently non-conductive, the utilization of humid air can enhance the overall conductivity, thereby making classification by dielectrophoresis possible. (Wang, et al. 2005)

The electric field is generated by a function generator SDG 1032X (Siglent Technologies co. Ltd) and subsequently magnified through a high voltage amplifier (Model 609A, Trek, Inc., Medina, NY) to achieve the amplitudes of high voltage of 0,8 kV to 4 kV. The waveform of the signal is a square, and the frequency is kept at 50 Hz.

Figure 15 illustrates the experimental setup for the experiment, as it displays all of the components needed to perform classification of the fibers.

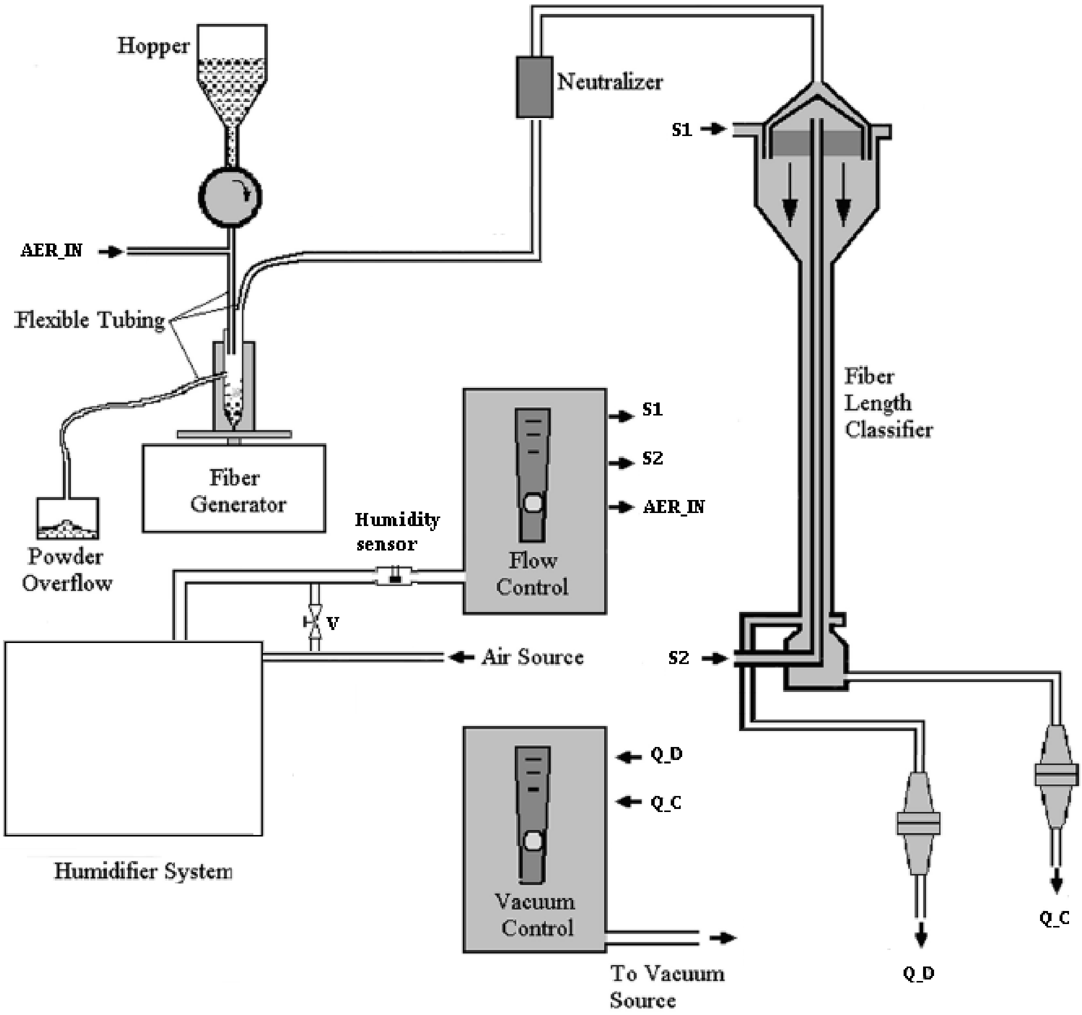

Figure 15: Schematic diagram of classification system (modified from Wang et al. 2005)

Figure 16 shows the photograph of the connected apparatus as it was used for experimental measurements in the laboratory.

Figure 16: Photograph of the classification system

6.3 Sample evaluation

The experimental measurement was set to take two minutes. The time was proven to be sufficient to collect a sufficient amount of fibers to evaluate if the fibers were classified without overloading the filter. The classified aerosol flow Q_C was captured on mixed cellulose ester filters MCE Millipore with a size of 25 mm in diameter. The samples were cleared by placing the filters on the microscoping glass, and the filter was melted by heated acetone vapours from the QuickFix acetone vaporizer. In the same way were cleared the samples from the dump flow Q_D were cleared for comparison. To ensure visibility of glass fibers, the PCM method must have been used as described in Chapter 4.1. The fibers were counted manually using the phase contrast microscopy utilizing the Nikon Eclipse microscope and analyzed by using the Method 7400 (*NIOSH Manual of Analytical Methods (NMAM), Fifth Edition: ASBESTOS and OTHER FIBERS by PCM* 2019). The fibers were counted using the Walton Beckett graticule, which is included in one of the ocular lenses of the microscope. The PCM methodology, i.e., manual fiber counting, adjusted according to the fibers used, was based on the following rules:

- Every fiber longer than 5 μm lying within the prescribed area is counted.
- The fiber must have a length-to-diameter ratio equal to or greater than 3:1.
- If the fiber lies on the border of the prescribed area, it is counted as half of a fiber if it meets the first two conditions.
- A fiber crossing the boundary more than once is not counted.
- All other fibers outside the prescribed area are disregarded.
- Fiber bundles are counted as one if individual fibers cannot be distinguished by observing both ends of the fiber.
- Counting stops when 100 fibers have been counted, with at least 20 areas examined. The count stops at 100 graticule areas regardless of the fiber count.

According to the method is necessary to select the observed areas randomly, however, the area of the filter should be covered as a whole. Each area should be observed for at least 15 seconds for accurate counting. To guarantee that all fibers are counted, it is crucial that all focal planes are scanned by the fine focus adjustment to identify very fine fibers that are embedded in the filter. It is not recommended to count at the edges of the filter. Total fiber count on filter is calculated by Equation (31)

$$F_i = \frac{A_i C_i}{a_i n_i} \tag{31}$$

where A_i is the area of the whole filter, C_i is the number of counted fibers, a_i is the area of the Walton-Beckett graticule, n_i is the number of counted areas.

Table 1: Filter areas

Filter diameter [mm]	**Diameter of effective surface area [mm]**	**Effective filter area [mm^2]**
25	21,7	368,8

Table 1 displays the filter areas that were used in Equation (31). The values were adopted from Kánska (2024). All filters were observed at the magnitude of 40x, therefore the area of Walton-Beckett graticule a_i was 0,071 mm^2 and the number of areas n_i was always 20. The variable value was just the number of fibers on the filter.

However, while the method was originally designed for fiber counting, the aim of the thesis was to classify fibers according to their dimensions. Therefore following experiments require the analysis not only of the count but also of the length of the fibers, which signifies the utilization of the Walton-Beckett graticule for length measurement of the fibers. The fibers were grouped into discrete length categories, as this method provided greater time efficiency compared to measuring each fiber individually, which would have been excessively labor- intensive. The primary length categories for analysis were 10, 15, 20, 30, 40, 50, and 60 μm. Conducting precise measurements of each individual fiber would be prohibitively time-consuming; therefore, the use of predefined length categories was adopted as a practical alternative. The diameter of all fibers is averaged to be 3 μm. There was a minimal amount of thinner fibers, which were omitted from the count. Figure 17 displays a sample from the fiber in the primary storage.

The photograph was taken by an Atik 320E (Atik Cameras Unipessoal Lda.) camera that is mounted on top of the microscope and provides black and white pictures from the microscope´s field of vision.

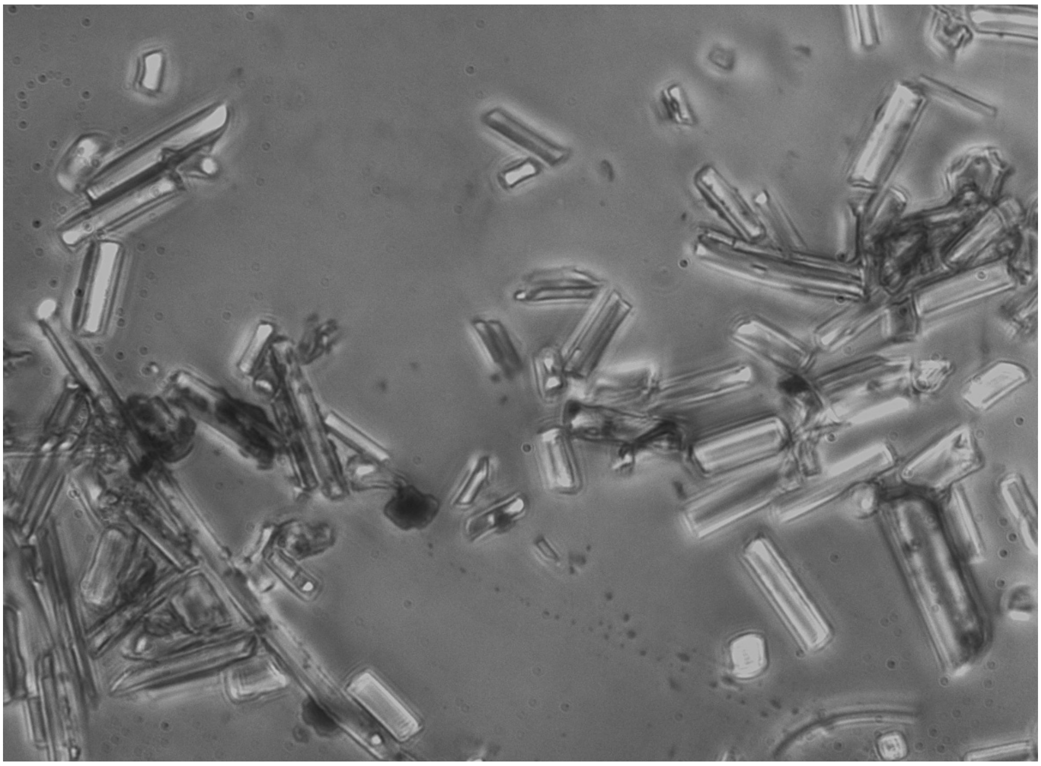

Figure 17: Sample photograph of unclassified fibers

7 Results

The measurement was focused on evaluation of the influence of multiple different input parameters on fiber classification. The key observed variables were:

- Relative humidity of the carrier gas,
- Flow rate ratio between sheath and aerosol flows,
- Applied voltage.

The aim of this thesis was to characterize the interdependent effects on dielectrophoretic fiber separation.

7.1 Relative humidity of the airflows

Classification of fibers based on their length is based on the dielectrophoretic principle, meaning that the electrical conductivity of fibers is a critical condition for classification to happen. Glass fibers are naturally non-conductive. However, glass fibers are capable of absorbing water by exposure to a humid environment, such as being in an airflow with controlled humidity. (Wang et al.2005)

The experimental investigation examined fiber classification performance across varying carrier gas humidity conditions. Figure 18 illustartes that the laboratory air supply was bifurcated into two parallel streams:

- Humidified pathway utilizing a water-contact humidification chamber,
- Bypass line.

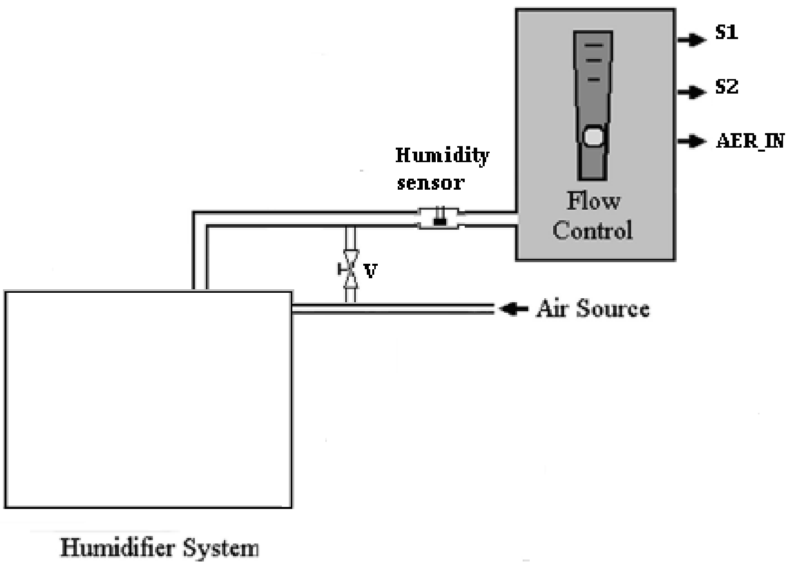

Figure 18: Humidifing system (modified from Wang et al. 2005)

The relative humidity of the combined flow was precisely regulated within a 10 to 50% range through proportional control of the bypass valve, monitored in real-time by an Arduino-based humidity monitoring system (https://www.arduino.cc). All trials were conducted under constant electrical parameters (3.5 kV, 50 Hz square wave excitation), with flow partitioning ratios maintained according to the configurations specified in Table 2.

Table 2: Airflow distribution

S1 [l/min]	S2 [l/min]	AER_IN [l/min]	Q_C [l/min]	O_D [l/min]
4	4	2	2	8

The classification became viable with relative humidity above 25%. Although the optimal conditions were achieved with relative humidity above 40%. Figure 19 displays the experimental data. The results imply that the minimum conductivity requirements are above 25% RH.

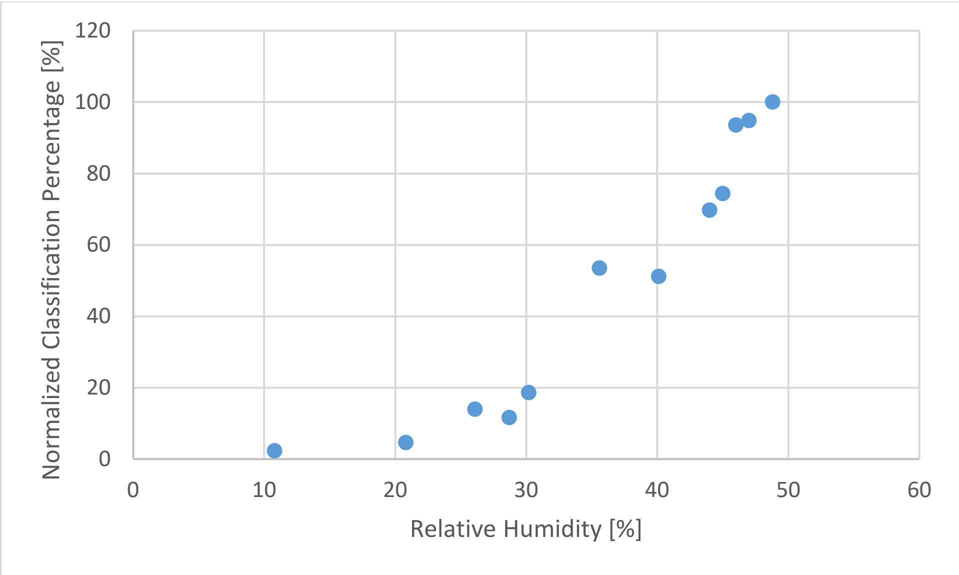

Figure 19: Humidity of carrier gas and classification percentage

7.2 Ratio of the airflows

The classification efficiency is influenced by the flow ratios, especially the ratio of inner sheath flow S1 to aerosol flow AER_IN. Experiments were conducted at a voltage of 4 kV. The adjustment to the parameters was made to the flows of inner and outer sheath flow simultaneously, while the aerosol flow was varied independently.

The experiment was conducted at 4 kV, with the relative humidity left unregulated, maintaining ambient levels of approximately 35%. The inner sheath flow and aerosol flow were configured according to the specifications in Table 3, while the outer sheath flow was consistently set equal to the inner sheath flow.

Table 3: Airflows of the sheath and aerosol flow

S1 [l/min]	3	3	4	4
AER_IN [l/min]	1	1,5	1,5	2

The experiment showed that reducing the inner sheath flow was not an effective way to collect shorter fibers. Lowering the flow did not lead to noticeably shorter fibers, and there was no clear increase in the number of shorter fibers in the distribution.

The overall flow rate through the classifier significantly influences the fiber output characteristics. Under standard operating conditions, totaling 10 l/min, a detailed evaluation is provided in Table 4.

Table 4: Airflow distribution

S1 [l/min]	S2 [l/min]	AER_IN [l/min]	Q_C [l/min]	O_D [l/min]
4	4	2	2	8

The amplitude of the aerosol airflow through the clafsiffier influnced the count of classified fibers. This proportional relationship demonstrates the direct dependence of fiber output on the system's flow conditions. The dependance of the fiber count on the airflow is illustarted in Figure 20.

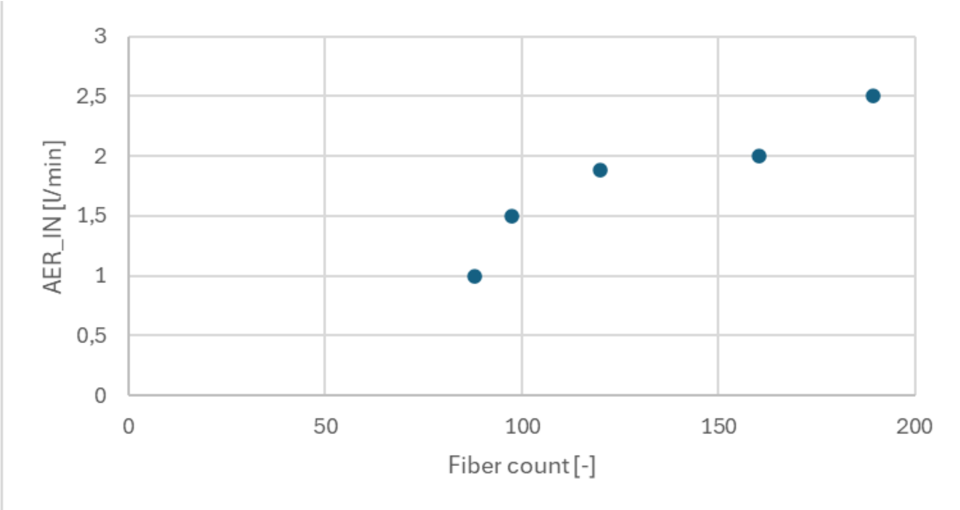

Figure 20: Fiber count dependent on aerosol airflow

7.3 Voltage

Dielectrophoric classification is strongly dependent on the voltage of the electric field, considering that dielectrophoresis is defined as the movement of an uncharged particle induced by a nonuniform electric field. The voltage was controlled using a function generator, with initial increments of 1 kV, followed by finer adjustments of 0.2 kV. Measurements were conducted under an average humidity of 45%, and the flow system remained consistent with the configuration previously outlined in Table 2.

The length of the fiber played a crucial role in determining the amount of charge generated on the surface of the fiber, thereby influencing the electric field strength required to induce motion and facilitate classification, as discussed in Chapter 5.2.

The applied voltage intervals of 1 kV demonstrated a significant effect on the classification length of the fiber. The results of measurements conducted at varying voltages are presented in Table 5. An inverse relationship was observed between the applied voltage and the classified fiber length, with higher voltages yielding shorter fibers.

Table 5: Voltage and fiber length dependence

Voltage [kV]	1	2	3	4
Length [µm]	50	30	15	10

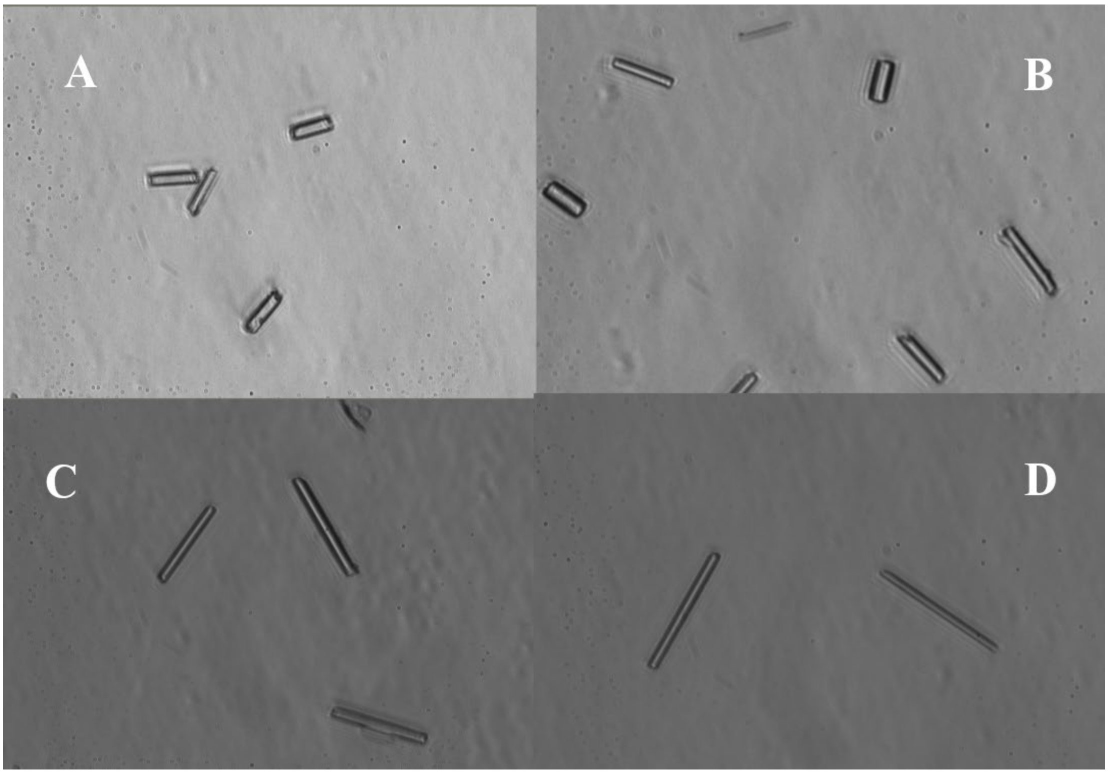

Figure 21: Classified fibers by voltage: A: 4 kV,B: 3 kV , C:2 kV, D: 1 kV

Table 5 presents the fiber length distribution in response to incremental adjustments in the applied voltage. The primary objective of this analysis was to determine the specific voltage thresholds that induce measurable changes in classified fiber length. Initial measurements with voltage steps of 1 kV, especially 1 to 2 kV, revealed substantial disparities in classified lengths, which can be seen in Figure 21. To achieve a more precise categorization of fiber lengths, subsequent measurements were conducted with a reduced voltage increment of 0,2 kV. This finer resolution allowed for a detailed assessment of the relationship between applied voltage and classified fiber length, enabling the identification of distinct length categories with greater accuracy. The resulting data, shown in Table 6, illustrates the relationship between applied voltage and classified fiber length at finer resolution. As shown in Figure 22, the fiber classification results demonstrate improved resolution when using smaller voltage increments (0,2 kV), enabling more precise classification of fiber length categories.

Table 6: Voltage and length dependence with finer adjustments

Voltage [kV]	0,8	1,2	1,4	1,5	1,6	1,8
Length [µm]	60	40	30	30	30	30

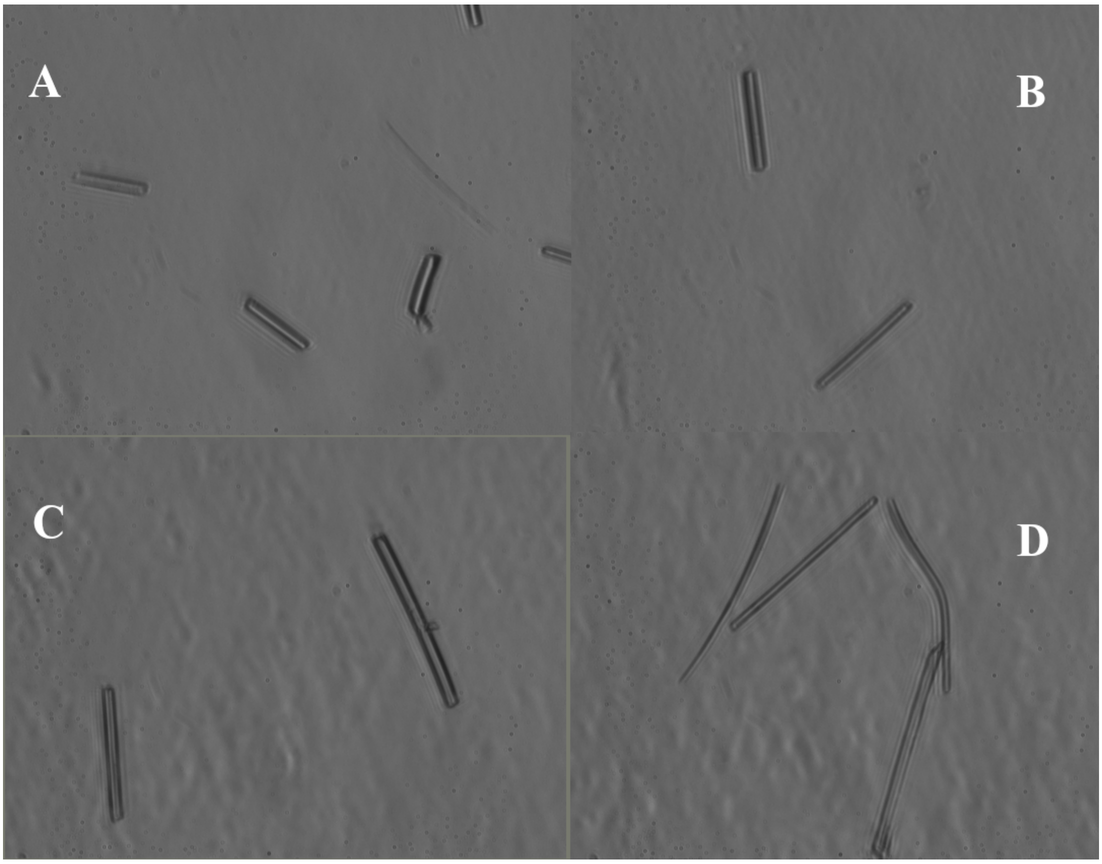

Figure 22: Classified fibers by voltage: A: 1,8 kV, B: 1,5 kV, C: 1,2 kV, D:0,8 kV

Figure 23 illustrates the dependece of classified length on the apllied voltages.

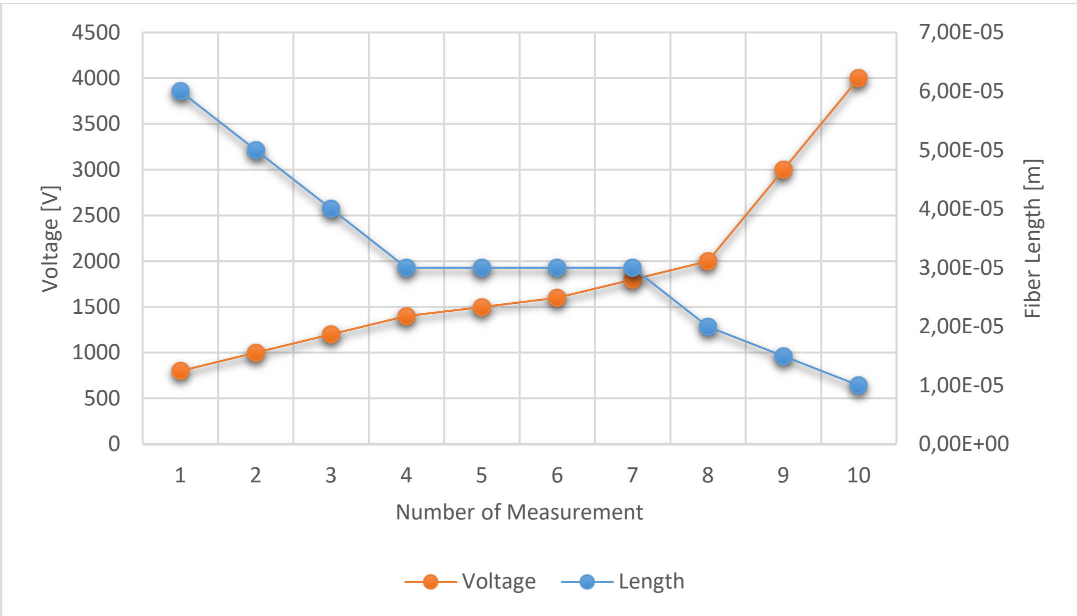

Figure 23: Graph of voltage-length dependence

8 Discussion

The experimental part of this thesis focuses on the classification of fibrous aerosol by utilizing the dielectrophoretic force exerted onto glass fibers, which moved through the nonhomogeneous electric field.

The observed fibers after classification were categorized into discrete length groups, as this approach offered optimal time efficiency compared to individual fiber measurements with the Walton-Beckett graticule, which would have been prohibitively labor-intensive. This methodology aligns with the work of Wang et al. (2005), who similarly utilized length-based categorization for fiber classification. The grouped classification proved effective for distinguishing fibers by length, as the observed length distribution did not exhibit continuous variation.

The classification efficiency of fibers is fundamentally dependent on their electrical conductivity properties. Glass being inherently insulating material, meaning that glass fibers should not be classifiable under the effects of the nonhomogeneous electric field. However, the majority of airborne particles can generally be regarded as conductive, primarily due to the adsorption of water on their surfaces (Fuchs, Davies 1989). Lilienfeld (1985) argued that all fibrous particles at ambient relative humidity above 30% are conductive, resulting from surface water adsorption. It was experimentally demonstrated that glass fibers with dimensions, 2 µm in diameter, 10–20 µm in length, exhibited conductive behavior when exposed to ambient relative humidity levels exceeding 30% within an AC field. (Lilienfeld 1985)

Wang et al. (2005) investigated the influence of humidity on the dielectrophoretic classification of both conductive carbon fibers and non-conductive glass fibers. They confirmed that increased humidity levels in the carrier gas had a negligible impact on the classification efficiency of conductive carbon fibers, as expected due to their inherent conductivity. In contrast, non-conductive glass fibers required a minimum relative humidity of 15% in the airflow to achieve effective classification. The authors attributed this humidity dependence to the formation of a conductive surface layer through multilayer water adsorption, which mobilizes ions and enhances the overall conductivity of micrometer-sized particles. (Wang et al. 2005)

The dielectric constant of glass exhibits minimal variation with frequency, showing less than a 5% difference across a range of 500 Hz to 1 MHz. However, the presence of a thin adsorbed water film on insulating particles can significantly alter their electrical behavior. When the adsorbed water film thickness is significantly smaller than the particle diameter, the system exhibits behavior analogous to a conductive-shelled dielectric sphere. Under these conditions, the interfacial conductivity dominates the particle's effective dielectric response. It is proposed that even a 10 nm thick adsorbed film can elevate the relative permittivity of a 1 µm glass bead to 15,000 under a 50 Hz AC field, demonstrating the profound impact of surface conductivity on insulating particles. The change in the conductivity is attributed to surface ions that are present in the water film and move along the surface. The ions present in the water film are attributed to originate from soluble substances leached from the glass surface. (Wang et al. 2005)

The influence of relative humidity on fiber classification was systematically investigated by incrementally adjusting the humidity levels of the carrier gas. Experimental results demonstrated that fiber classification became feasible at RH levels exceeding 25%, while optimal classification performance was achieved at RH values above 40%.

The results showed a general consistency with Lilienfeld (1985). Although data obtained by Wang et al. (2005) reported classification viable from RH 15%, the difference may be attributed to time of fibers spend in humidified air, as their setup included additional ageing chamber, where fibers were exposed to humidied air for an extened period of time.

The yield of classified fibers exhibits linear dependence on the amount of aerosol airflow input. Increased airflow provides highly sufficient yield for data evaluation, however decrease in the aerosol airflow by 30% displays less overloaded filter for evalution, meaning that it can be analyzed more efficiently. The utilization of classifier and its capabilities at lowered overall airflow does not skew the results. The utilization of the classified airflow for subsequent use in other experiments, that require fibrous aerosols with monodisperse lengths, at any required airflow is possible.

Deye et al. (1999) demonstrated that the inner sheath flow significantly affects the minimal classifiable fiber length in dielectrophoretic classification. Their experiments revealed that positioning the aerosol flow closer to the inner electrode, while maintaining a lower inner sheath flow, leads to broader fiber length distributions. This highlights a critical trade-off: reducing the inner sheath flow minimizes fiber length but simultaneously increases length dispersion. Additionally, the study examined the influence of flow ratios, specifically the aerosol-to-classified flow ratio, on classification performance. The results indicated that the length spread of fibers does not scale proportionally with increasing classified flow to the stable input aerosol flow, as classification is primarily governed by dielectrophoretic forces, where fiber length remains the dominant factor in separation efficiency. (Deye et al. 1999)

The experiment revealed that the reduction of the inner sheath flow did not provide a viable method for obtaining shorter fibers. Lowering the inner sheath flow to obtain shorter fibers was not plausible. The length distribution with a smaller inner sheath flow was not proven to increase. The disagreement with the study done by Deye et al. (1999) may be attributed to the relative humidity of the carrier gas, as the classification was done at the lowest viable humidity. The other possible point of the disagrement may be the operational limitation can be attributed to dimensions of the fibers. Also, the approach to categorize the fibers into length groups, where the shortest length group already includes the shortest particles that can be classified as a fiber. The classification process was further constrained by the inherent physical dimensions of the glass fibers under investigation. As stated in Chapter 3.1, a particle must maintain a minimum fibrocity β of 3 to be properly characterized as a fiber. The glass fibers, utilized in this experiment, possessed a nominal diameter of 3 μm, which consequently imposed a fundamental lower limit of 9 μm on classifiable fiber lengths. Secondly, a clear threshold behavior was demonstrated, wherein the minimum classifiable fiber length was achieved at an applied voltage of 4 kV. Beyond this operational point, neither further reduction of the inner sheath flow rate nor additional increases in applied voltage yielded measurable improvements in the classification of shorter fibers.

The observed variation in voltage dependence can be explained by Equation (11), where the only variables are fiber length, applied voltage, and functions of the fibrocities, while all other parameters, such as the material properties of the glass fibers and the surrounding environment, remain constant across all calculations. Experimental results support this relationship, demonstrating an inverse proportionality between the classified fiber length and the applied voltage, as illustrated in Figure 23.

In the study conducted by Wang et al. (2005), the observed fibers exhibited an average diameter of approximately 1 μm, which is three times smaller than those examined in the present experiment. Nevertheless, the applied voltages in both studies are in agreement, a finding that can be explained by Equation (13), where fiber diameter can be neglected, and length remains the sole determining factor. Which was the assumption made by Lipowicz, Yeh (1989) for fibers with $\beta > 5$, and they argued that the deviation between Equation (13) and Equation (11) is negligible, and the Equations (11) and (13) exhibit strong agreement between them.

In their experimental work, Wang et al. (2005) established specific relationships between applied voltages and corresponding fiber length classifications. Their results demonstrated that an applied voltage of 4 kV consistently classified fibers measuring 10 μm in length, while a lower voltage of 1.52 kV was associated with longer fibers of 30 µm. These particular findings corresponded with the measurement in this thesis. However, Wang et al. (2005) were also able to classify even shorter fibers of the length 5 µm through application of a higher voltage with the magnitude of 6.56 kV. As mentioned before, the fibers used in this study had a diameter of 3 µm, meaning that if they were only 5 µm long, they would not classify as fibers, as those dimensions would not qualify as fibers, as the aspect ratio fails to meet the minimum requirements of $\beta > 3$.

The objective of this experimental investigation was to determine whether systematically varying the applied voltage would produce correspondingly gradual changes in the classified fiber lengths. The measurements revealed distinct voltage thresholds for fiber classification, as clearly demonstrated in Table 5. Notably, voltage increments of 1 kV resulted in discrete, step like transitions between different classified length categories. Subsequent measurements focused specifically on examining if more refined voltage variations might produce gradual transitions in the classification outcomes. However, as presented in Table 6, the results indicated that voltage adjustments within the range of 1.4 kV to 1.8 kV consistently yielded identical classification outcomes, with all measurements corresponding to fibers of 30 µm length. One possible explanation is that within the voltage range of 1.4 to 1.8 kV, the induced charge on the fibers reaches a sufficient threshold to consistently classify them into the 30 µm category. However, since the fiber lengths were categorized into discrete groups, a continuous relationship between applied voltage variations and classified lengths was not observed. It is plausible that a more comprehensive measurement approach, one not constrained by predefined length categories, might have revealed a gradual progression in fiber lengths. Such analysis could potentially have identified intermediate classifications, such as fibers measuring 25 µm or 35 µm in length, thereby demonstrating finer gradations in the voltage-length relationship. Regardless, more pronounced changes in fiber length classification were observed with relatively small voltage adjustments in other ranges. As illustrated in Figure 23, a voltage difference of only 600 V resulted in a classification shift from 60 µm to 30 µm. In contrast, for the smallest classified lengths 10 to 20 µm, a larger voltage difference of 2 kV was required to produce a comparable transition. This behavior suggests that the relationship between voltage and classified fiber length follows a quadratic dependence, consistent with the mathematical formulation presented in Equation (13).

This thesis demonstrates that dielectrophoretic classification can be effectively applied to non-conductive fibrous materials, enabling the generation of monodisperse aerosol. While experimental validation was conducted using glass fibers, the underlying principles suggest this method could be extended to polymer fibers of varying chemical compositions. Moreover, even bioerodible polymers utilized in many biomedical applications (Thieme et al. 2011), could be classified by dielectrophoresis.

The production of fibrous aerosol with fibers of classified lengths may potential use in a medical field. Recently, there has been an effort to explore the option of drug delivery to the lungs in the form of inhaled fibers. Spherical particles with a diameter larger than 5µm are often filtered in the extrathoracic airways. However, fibers exceeding the length of 200 µm have been found in the lungs. Fibers provide a significant advantage for the delivery of pharmaceuticals compared to more spherical particles. The drug payloads can be precisely localized to specific lung regions, by controlling the dimension of the fiber by optimizing the dosage, therefore also influencing the mass of the fiber. (Gilbertson et al. 2005)

In drug delivery applications, nanostructures such as nanorods, nanotubes, and nanofibers are emerging as promising carriers for targeted transport and controlled release. These materials enable a shift from systemic to locoregional therapy, enhancing therapeutic precision while minimizing off-target effects. The high aspect ratio of fibers and aerodynamic properties allow deeper alveolar deposition and reduced exhalation losses, significantly increasing the effective drug dose delivered to pulmonary tissues. (Thieme et al. 2011) The length of the fibers utilized in inhaltion therapy must be controlled, the production of fibers must ensure the monodisperse length, and subsequent classification of the fibers can serve as a control of the length.

Monodisperse fibrous aerosol can be utilized in laboratory settings for further analytical experiments that would benefit from controlled input of fibrous aerosols. Mainly for controlled exposure studies, where precise length distribution of fibers in the aerosol could enable a more focused study of deposition in the pulmonary system. Monodispersed fibrous aerosol could be utilized as standardized reference materials for calibrating particle counters, spectrometers, and other analytical devices. Another field of use could be filtration testing, where monodispersed aerosols would provide an interesting approach (Arefin et al. 2017).

9 Conclusion

This master's thesis investigated the processes involved in the preparation, generation, measurement, classification, and filtration of fibrous aerosols. The theoretical section provided a definition of fibrous aerosols and fibers, along with an analysis of fiber morphology and its influence on aerodynamic behavior. The following chapter examines the formation of fibers through various techniques and diverse chemical compositions, ranging from polymers to metals. Special emphasis is placed on electrospinning, a widely used method for producing fibers with applications in the medical field, especially, on the formation of short fibers from electrospun fibers, which could find their utilization in inhalable drug delivery systems. The health effects of fiber exposure have been extensively studied for decades. However, with the continuous development of novel carbon nanofibers, comprehensive safety measures must be established to ensure proper health protection. The following chapter examines approaches based on microscopy for fiber observation, analyzing various techniques to ensure comprehensive fiber detection and prevent oversight of fibers. Fiber classification methods are categorized into two primary groups: diameter-based and length-based separation. While both approaches are recognized, this thesis focuses principally on length classification methodologies. These techniques utilize the electrical properties of airborne fibers to achieve precise size classification, with particular emphasis on dielectrophoretic separation principles.

The experimental part of this study focuses on the dielectrophoretic classification of glass fibers, examining both the classification process itself and the influence of key input parameters on classification quality. A systematic approach was implemented, beginning with the preparation of glass fiber samples, followed by a detailed description of the experimental system and its components. The experimental design builds upon previous research while specifically addressing fibers within defined morphological parameters. By maintaining control over experimental conditions and fiber specifications, this work establishes a direct correlation between operational parameters and classification efficiency. Previous studies of classification served as a motivation for further and comprehensive analysis of dielectroporetic classification. The results of this thesis confirm the necessary utilization of humidified airflow for the classification of non-conductive fibers. The applied voltage directly affects the length range of the classified fibers, and the magnitude of the voltage is the same for the fibers with the same length and different diameters.

The limitations of this study lie in the classification of fibers into length categories, a method chosen due to time efficiency. Additionally, the approach used was developed solely on counting fibers, and to obtain valuable results for this measurement required manual verification of their lengths during evaluation. Measuring the length of each individual fiber would have required a different method, as simple counting with the Walton-Beckett graticule was insufficient. Consequently, it was not possible to calculate the deviation from the average length for the classified fibers. Despite this limitation, the study yielded satisfactory results that were comparable to previous studies. The findings of this study may find further application in the classification of other non-conductive fibers.

BIBLIOGRAPHICAL REFERENCES

AREFIN, Amit Md. Estiaque, MASUD, M.H., JOARDDER, Mohammad U.H. and AKHTER, Md. Shamim, 2017. A monodisperse-aerosol generation system: Design, fabrication and performance. *Particuology*. Online. October 2017. Vol. 34, p. 118–125. DOI 10.1016/j.partic.2017.03.005. [Accessed 19 May 2025].

ASGHARIAN, Bahman, 1999. Size Separation of Spherical Particles and Fibers in an Aerosol Centrifuge. *Aerosol Science and Technology*. Online. April 1999. Vol. 30, no. 4, p. 383–400. DOI 10.1080/027868299304570. [Accessed 28 February 2025].

BARON, P. A., DEYE, G. J. and FERNBACK, J., 1994. Length Separation of Fibers. *Aerosol Science and Technology*. Online. January 1994. Vol. 21, no. 2, p. 179–192. DOI 10.1080/02786829408959707. [Accessed 29 May 2024].

BARON, Paul A., 2001. Measurement of Airborne Fibers: A Review. *INDUSTRIAL HEALTH*. Online. 2001. Vol. 39, no. 2, p. 39–50. DOI 10.2486/indhealth.39.39. [Accessed 9 February 2025].

BERGMANN, Melanie, MÜTZEL, Sophia, PRIMPKE, Sebastian, TEKMAN, Mine B., TRACHSEL, Jürg and GERDTS, Gunnar, 2019. White and wonderful? Microplastics prevail in snow from the Alps to the Arctic. *Science Advances*. Online. 2 August 2019. Vol. 5, no. 8, p. eaax1157. DOI 10.1126/sciadv.aax1157. [Accessed 14 March 2025].

BEZEMER, Gerrit, 2006. *Cobalt supported on carbon nanofibers as catalysts for the Fischer-Tropsch synthesis.* Universiteit Utrecht. ISBN 90-393-4133-8.

CHEN, B. T., YEH, H. C. and HOBBS, C. H., 1993. Size Classification of Carbon Fiber Aerosols. *Aerosol Science and Technology*. Online. January 1993. Vol. 19, no. 2, p. 109–120. DOI 10.1080/02786829308959625. [Accessed 24 February 2025].

DEYE, G. J., GAO, P., BARON, P. A. and FERNBACK, J., 1999. Performance Evaluation of a Fiber Length Classifier. *Aerosol Science and Technology*. Online. May 1999. Vol. 30, no. 5, p. 420–437. DOI 10.1080/027868299304471. [Accessed 27 January 2025].

EVANS, Douglas E. and KI, Ku Bon, 2010. Aerosol Monitoring during Carbon Nanofiber Production: Mobile Direct-Reading Sampling. *The Annals of Occupational Hygiene*. Online. 6 May 2010. DOI 10.1093/annhyg/meq015. [Accessed 23 January 2025].

EVANS, Douglas E. and TURKEVICH, Leonid A., 2012. Dustiness of Fine and Nanoscale Powders. *The Annals of Occupational Hygiene*. Online. 12 October 2012. DOI 10.1093/annhyg/mes060. [Accessed 23 January 2025].

FUCHS, N. A. and DAVIES, C. N., 1989. *The mechanics of aerosols*. Rev. and enl. ed. New York: Dover Publications. ISBN 978-0-486-66055-4.

GASCOYNE, Peter and SHIM, Sangjo, 2014. Isolation of Circulating Tumor Cells by Dielectrophoresis. *Cancers*. Online. 12 March 2014. Vol. 6, no. 1, p. 545–579. DOI 10.3390/cancers6010545. [Accessed 5 February 2025].

GILBERTSON, K.E., FINLAY, W.H., LANGE, C.F., BRETT, M.J., VICK, D. and CHENG, Y.S., 2005. Generation of fibrous aerosols from thin films. *Journal of Aerosol Science*. Online. July 2005. Vol. 36, no. 7, p. 933–937. DOI 10.1016/j.jaerosci.2004.10.010. [Accessed 27 January 2025].

GOLDMANN, Eryk, GÓRSKI, Marcin and KLEMCZAK, Barbara, 2021. Recent Advancements in Carbon Nano-Infused Cementitious Composites. *Materials*. Online. 9 September 2021. Vol. 14, no. 18, p. 5176. DOI 10.3390/ma14185176. [Accessed 13 May 2025].

GREINER, Andreas and WENDORFF, Joachim H., 2007. Electrospinning: A Fascinating Method for the Preparation of Ultrathin Fibers. *Angewandte Chemie International Edition*. Online. 23 July 2007. Vol. 46, no. 30, p. 5670–5703. DOI 10.1002/anie.200604646. [Accessed 22 March 2025].

HAN, R. J., MOSS, O. R. and WONG, B. A., 1994. Airborne Fiber Separation by Electrophoresis and Dielectrophoresis: Theory and Design Considerations. *Aerosol Science and Technology*. Online. January 1994. Vol. 21, no. 3, p. 241–258. DOI 10.1080/02786829408959713. [Accessed 9 April 2025].

HINDS, William C. and ZHU, Yifang, 2022. *Aerosol technology: properties, behavior, and measurement of airborne particles*. Third edition. Hoboken, NJ: Wiley. ISBN 978-1-119-49404-1.

IGLESIAS, Francisco J., SANTAMARÍA, Carlos, LÓPEZ, M. Carmen and DOMÍNGUEZ, Angel, 1989. Dielectrophoresis. In: NEUMANN, Eberhard, SOWERS, Arthur E. and JORDAN, Carol A. (eds.), *Electroporation and Electrofusion in Cell Biology*. Online. Boston, MA: Springer US. p. 37–57. ISBN 978-1-4899-2530-5. [Accessed 31 January 2025].

KÁNSKA, Jana, 2024. *Mechanika proudění inhalovaných vláken v modelu plic*. Online. Brno: Vysoké učení technické v Brně, Fakulta strojního inženýrství, Energetický ústav. Vedoucí práce František Lízal. Available from: https://www.vut.cz/studenti/zav-prace/detail/157450

KU, Bon Ki and BIRCH, M. Eileen, 2019. Aerosolization and characterization of carbon nanotube and nanofiber materials: Relationship between aerosol properties and bulk density. *Journal of Aerosol Science*. Online. January 2019. Vol. 127, p. 38–48. DOI 10.1016/j.jaerosci.2018.10.004. [Accessed 25 January 2025].

KULKARNI, Pramod (ed.), 2011. *Aerosol measurement: principles, techniques, and applications*. 3. ed. Hoboken, NJ: Wiley. ISBN 978-0-470-38741-2.

LI, Yaowei, SHAO, Longyi, WANG, Wenhua, ZHANG, Mengyuan, FENG, Xiaolei, LI, Wenjun and ZHANG, Daizhou, 2020. Airborne fiber particles: Types, size and concentration observed in Beijing. *Science of The Total Environment*. Online. February 2020. Vol. 705, p. 135967. DOI 10.1016/j.scitotenv.2019.135967. [Accessed 29 May 2024].

LILIENFELD, Pedro, 1985. Rotational electrodynamics of airborne fibers. *Journal of Aerosol Science*. Online. January 1985. Vol. 16, no. 4, p. 315–322. DOI 10.1016/0021-8502(85)90039-4. [Accessed 3 May 2025].

LIPOWICZ, Peter J. and YEH, Hsu Chi, 1989. Fiber Dielectrophoresis. *Aerosol Science and Technology*. Online. January 1989. Vol. 11, no. 3, p. 206–212. DOI 10.1080/02786828908959313. [Accessed 24 February 2025].

LIZAL, Frantisek, MALY, Milan, ELCNER, Jakub, FARKAS, Arpad, PECH, Ondrej, MISIK, Ondrej, JEDELSKY, Jan and JICHA, Miroslav, 2019. Dielectrophoretic classification of fibres: principles and application to glass fibres suspended in air. DANČOVÁ, P. and NOVOSAD, J. (eds.), *EPJ Web of Conferences*. Online. 2019. Vol. 213, p. 02053. DOI 10.1051/epjconf/201921302053. [Accessed 29 May 2024].

MYOJO, Toshihiko, 1999. A Simple Method to Determine the Length Distribution of Fibrous Aerosols. *Aerosol Science and Technology*. Online. January 1999. Vol. 30, no. 1, p. 30–39. DOI 10.1080/027868299304868. [Accessed 24 April 2025].

NIEMCZYK-SOCZYNSKA, Beata, DULNIK, Judyta, JEZNACH, Oliwia, KOLBUK, Dorota and SAJKIEWICZ, Pawel, 2021. Shortening of electrospun PLLA fibers by ultrasonication. *Micron*. Online. June 2021. Vol. 145, p. 103066. DOI 10.1016/j.micron.2021.103066. [Accessed 23 March 2025].

NIOSH Manual of Analytical Methods (NMAM), Fifth Edition: ASBESTOS and OTHER FIBERS by PCM, 2019. . National Institute for Occupational Safety and Health.

PANKRÁC, Vítězslav, 2020. Příklady I II: Elektrické pole. In: *Základy teorie elektromagnetického pole*. Online. ČVUT Praha. Available from: https://elmag.fel.cvut.cz/sites/default/files/users/pankrac/files/Priklady_I_II_elektricke_pole.pdf

PESCH, Georg R. and DU, Fei, 2021. A review of dielectrophoretic separation and classification of non-biological particles. *ELECTROPHORESIS*. Online. January 2021. Vol. 42, no. 1–2, p. 134–152. DOI 10.1002/elps.202000137. [Accessed 16 November 2024].

ROBBIE, K. and BRETT, M. J., 1997. Sculptured thin films and glancing angle deposition: Growth mechanics and applications. *Journal of Vacuum Science & Technology A: Vacuum, Surfaces, and Films*. Online. 1 May 1997. Vol. 15, no. 3, p. 1460–1465. DOI 10.1116/1.580562. [Accessed 24 March 2025].

ROOD, A. P., WALKER, E. J. and MOORE, D., 1992. Construction of a Portable Fiber Monitor Measuring the Differential Light Scattering from Aligned Fibers. *Aerosol Science and Technology*. Online. January 1992. Vol. 17, no. 1, p. 1–8. DOI 10.1080/02786829208959555. [Accessed 6 March 2025].

SAWAWI, Marini, WANG, Ting Yi, NISBET, David R. and SIMON, George P., 2013. Scission of electrospun polymer fibres by ultrasonication. *Polymer*. Online. July 2013. Vol. 54, no. 16, p. 4237–4252. DOI 10.1016/j.polymer.2013.05.060. [Accessed 25 March 2025].

SPURNY, Kvetoslav R., 1999. *Analytical Chemistry of Aerosols: Science and Technology*. 1st ed. London: CRC Press. ISBN 978-1-56670-040-5.

THIEME, Marcel, AGARWAL, Seema, WENDORFF, Joachim H. and GREINER, Andreas, 2011. Electrospinning and cutting of ultrafine bioerodible poly(lactide-co-ethylene oxide) tri- and multiblock copolymer fibers for inhalation applications. *Polymers for Advanced Technologies*. Online. September 2011. Vol. 22, no. 9, p. 1335–1344. DOI 10.1002/pat.1617. [Accessed 17 March 2025].

VERRECK, Geert, CHUN, Iksoo, PEETERS, Jef, ROSENBLATT, Joel and BREWSTER, Marcus E., 2003. Preparation and Characterization of Nanofibers Containing Amorphous Drug Dispersions Generated by Electrostatic Spinning. *Pharmaceutical Research*. Online. 1 May 2003. Vol. 20, no. 5, p. 810–817. DOI 10.1023/A:1023450006281.

WANG, Zuocheng, HOPKE, Philip K., BARON, Paul A., AHMADI, Goodarz, CHENG, Yung-Sung, DEYE, Gregory and SU, Wei-Chung, 2005. Fiber Classification and the Influence of Average Air Humidity. *Aerosol Science and Technology*. Online. November 2005. Vol. 39, no. 11, p. 1056–1063. DOI 10.1080/02786820500380198. [Accessed 4 June 2024].

LIST OF SYMBOLS AND ABBREVAITIONS

Symbol	Name	Unit
a	Radius of a homogenous spherical particle	[m]
a_i	Area of Walton-Becket graticule	[mm^2]
A_i	Area of the whole filter	[mm^2]
c	Constant dependent on the electrode size and spacing and insulation thickness and material	[-]
Ci	Concentration of fiber type i	[#/ml]
C_i	Number of counted fibers	[-]
D	Diameter of fiber	[µm]
d_a	Aerodynamic diameter	[µm]
d_{eff}	Effective filter diameter	[mm]
d_f	Physical diameter	[µm]
E	Electric field	[V/m]
F	Dielectric force	[N]
F_B	Area of the image field	[mm^2]
F_D	Drag force	[N]
F_{DEP}	Time averaged dielectric force	[N]
$\mathrm{F_i}$	Total fiber count on filter	[-]
K_m	Dielectric constant of an electrically insulating medium	[-]
L	Length of fiber	[µm]
N	Number of image fields examined	[-]
n_i	Number of fibers counted for fiber type *i*	[-]
n_i	Number of counted areas	[-]
r	Radial distance	[m]
$Rout$	Outer radius	[m]
Rin	Inner radius	[m]
t	Deposition time	[s]
U	Voltage	[V]
v	Velocity	[m/s]
V	Total sampled air volume	[ml]
V_B	Sampled air volume per field	[ml]
α	Ratio between the dielectric constant of the fiber and the insulating medium	[-]
β	Fibrocity	[-]
ϵ_0	Relative permittivity of vacuum	[F/m]
ϵ_m	Relative permittivity of medium	[-]
η	Dynamic viscosity	[m^2/s]
ρ_0	Standard fiber density	[kg/m^3]
ρ_f	Fiber density	[kg/m^3]
τ	Linear charge	[C/m]

$\chi_{\parallel}$	Parallel dynamic shape factors	[-]
$\chi_{\perp}$	Perpendicular dynamic shape factors	[-]

Symbol of dimensionless number	**Name of dimensionless number**
K_{CM}	**Clausius-Mossotti factor**
Re	Reynolds number
Re_p	Reynolds number for the particle

Abbreviation	**Meaning**
AC	Alternative current
AER_IN	Aerosol flow
CNFs	Carbon nanofibers
CNTs	Carbon nanotubes
DC	Direct current
EDX	Energy-dispersive X-ray
FAM	Fibrous Aerosol Monitor
GLAD	Glancing angle deposition
HPMC	Hydroxylpropylmethylcellulose
HRH	Human respiratory height
Kr	Krypton
MCE	Mixed cellulose ester
MMMFs	Man-Made Mineral Fibers
MWCNTs	Multi-walled carbon nanotubes
nDEP	Negative dielectric polarization
TEM	Transmission electron microscope
PAN	Poly(acrylonitrile)
PCM	Phase contrast light microscope
pDEP	Positive dielectric polarization
PLA-PEO-PLA	Poly(lactide-co-ethylene oxide)
PLLA	Poly(L-lactide)
PLM	Polarized light microscope
PMMA	Poly(methyl methacrylate)
PS	Polystyrene
RB	Roof of the building
RH	Relative humidity
S1	Sheath Flow 1
S2	Sheath Flow 2
SEM	Scanning electron microscope
SWCNTs	Single-walled carbon nanotubes
Q_C	Classified airflow
Q_D	Dump airflow
VBAG	Vibrating Bed Aerosol Generator

LIST OF FIGURES

LIST OF TABLES